Journal of Microelectronics and Electronic Packaging (2015) **12**, 189-204
Copyright © International Microelectronics Assembly and Packaging Society
ISSN: 1551-4897

Review of Devices, Packaging, and Materials for Cryogenic Optoelectronics

Eivind Bardalen,[1,*] Muhammad Nadeem Akram,[1] Helge Malmbekk,[2] and Per Ohlckers[1]

Abstract—**In this article, developments and techniques related to optical-fiber-coupled devices operating at cryogenic temperatures are reviewed. These devices include superconducting electronics and photodetectors. Superconducting circuits have a number of suitable characteristics in terms of speed and efficiency, lower power consumption, and traceability to fundamental quantum properties. Thus, applications are found in a number of technologies, such as communication and metrology. Often, the devices are coupled by an optical fiber link to an external source. A suitable design of the optical coupling at cryogenic temperatures entails considerations of electromagnetic behavior, geometry, components, material choices, and customized packaging schemes. Minimizing thermomechanical stresses and deformation is a challenge due to the extreme temperature span, from room temperature to below 10 K. Due to the thermomechanical properties at low temperatures, with high contraction and brittleness of some materials, careful design and testing is dictated for the method of mechanical attachment and alignment techniques to avoid failure. Solutions for the efficient, robust optical coupling remain a challenge for some of these devices.**

Keywords—**Packaging and interconnection, cryogenic operation, superconductive circuit, photodetector, photodiode, optical fiber, Josephson junction, single-quantum flux electronics**

Introduction

Superconducting devices, cooled to very low temperatures, typically below 10 K, have unique properties and may outperform semiconductor devices in terms of speed, sensitivity, and efficiency. For example, superconducting electronic circuits based on Josephson junctions have the potential of reaching high speeds, up to 100 GHz [1]. For such devices, an optical coupling from room-temperature sources to system, located at cryogenic temperature, is an interesting prospect for improving performance. Replacing electrical wirings, which have high capacitances and inductances and are sensitive to noise, with optical couplings has a number of benefits, such as reduced thermal load and better high-frequency characteristics.

Similarly, ultrasensitive photon detectors based on thin superconducting films have the potential of detecting single photons and resolving the number of photon in weak optical pulses, enabling various quantum optical technologies [2].

For the realization of these devices, an efficient optical coupling between single-mode fibers and the active area is crucial. The bonding and packaging of the fiber is a challenge, due to the thermal stresses developed near material interfaces when cooling down to cryogenic temperatures. Therefore, packaging aspects, such as choosing a design, materials, and components, are important for developing a robust, efficient system. In this review, we describe optically coupled superconducting devices, optical coupling techniques, and methods for interconnection and packaging of these devices In the last section, we discuss relevant material properties for some commonly used materials and bonding techniques.

Cryogenic Optoelectronic Devices

At cryogenic temperatures, superconducting phenomena can enable a range of devices with excellent characteristics. In addition, thermal fluctuations are suppressed, changing the characteristics and performance of many well-known devices. In practice, the superconducting state is achieved by cooling the devices to temperatures below 10 K, such as in a cryostat cooled by liquid helium to 4.2 K (e.g., [3]) or in cryogen-free coolers (e.g., [4]).

Development of high-speed optically coupled cryogenic devices may lead to practical applications in several technologies, such as communications, computing, and metrology. In general, the devices are characterized by small sizes, with active areas typically <30 μm in diameter, coupled to single-mode fibers. In the following, the development of some of these devices is briefly described.

A. Superconducting Photon Detectors

Highly sensitive photodetectors, with the ability to detect individual photons or the number of photons in a pulse, has applications in many fields, including quantum computing, communications, astronomy, and metrology. (see e.g., [5-7] and references therein). Recently, there has been an effort to develop optical sensors based on superconducting materials. Basically, the detection mechanism is due to the absorption of optical power in the superconducting material, which induces a phase shift to the normal state, followed by a subsequent recovery to the superconducting state, which can be detected by external circuitry.

Two notable examples of these are the following: nanowire single photon detectors (SNSPDs), as seen in Fig. 1, and transition edge sensors (TES). These detectors are fabricated as structures of thin layers, around 100 nm of superconducting

The manuscript was received on June 24, 2015; revision received on October 14, 2015; accepted on November 6, 2015
[1]Buskerud and Vestfold University College, Borre, Norway
[2]Norwegian Metrology Service, Kjeller, Norway
*Corresponding author; email: eivind.bardalen@hbv.no

doi:10.4071/imaps.485 1551-4897 © 2015 International Microelectronics Assembly and Packaging Society

Downloaded from http://meridian.allenpress.com/jmep/article-pdf/12/4/189/2245811/imaps_485.pdf by guest on 31 October 2022

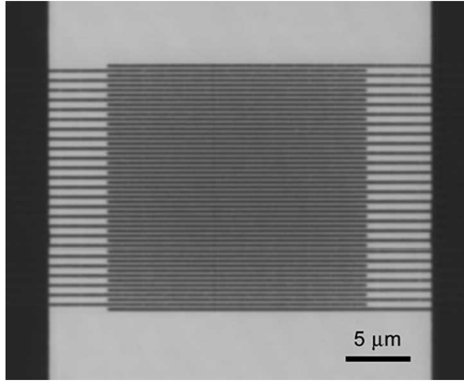

Fig. 1. An NbN SNSPD sensor on an MgO substrate. Reproduced from [8].

materials. Recently, an optical link between a moon orbiting satellite and an SNSPD sensor on earth have been demonstrated, with download data rates up to 622 Mbps [9].

The performance of these devices is described in terms of detection efficiency, recovery time, timing jitter, and dark count rates [2]. The efficiency of these detectors depends on the packaging and optical coupling from source to the detector, the intrinsic detection efficiency, and the external circuitry. According to [10], a useful equation describing this, the "system detection efficiency" can be written as:

$$\eta_{\mathrm{sde}} = \eta_{\mathrm{coupling}} \times \eta_{\mathrm{absorption}} \times \eta_{\mathrm{registering}} \quad (1)$$

The TES consist of a thin superconducting film operated in the narrow temperature region between the superconducting and normal state [11], typically a few hundred millikelvin. By applying a voltage bias over the detector in parallel to a shunt resistance, the temperature of the film can be kept near the superconducting transition through Joule heating. Absorption of a photon causes the temperature to increase, which leads to a change in resistance as the material is heated to above the equilibrium temperature to the normal state. The recovery to the normal state is due to heat flow to the substrate [12]. The pulse height of the current depends on the number of photons absorbed and is read by external circuitry, such as a SQUID (superconducting quantum interference device) array [13].

TES based on tungsten films were demonstrated to measure the number of photons in single pulses of light at a wavelength of 1,550 nm [14], though fiber alignment and surface reflection limited the detection efficiency to 20%. Later, the detection efficiency was improved to 95% by incorporating a backside reflecting mirror, antireflective (AR) layers, and precise alignment [5]. TES operation based on Ti/Au has been demonstrated for 690 nm and 1,310 nm [15], while a titanium-based TES [6] has been developed for 850 nm, with 98% detection efficiency achieved by directly coupling the optical fiber and incorporating AR layers and a dielectric mirror.

Although TES have very small dark count rates and low jitter, they are relatively slow, demonstrated with recovery times below 170 ns for small area sensors [16]. The high quantum efficiency photon-resolving capabilities, however, motivates research for applications in quantum technologies, such as quantum communications and quantum computing (see e.g., [5]). Furthermore, a fiber-coupled picowatt radiometer based on TES has been developed [7].

SNSPDs, similarly, are based on a phase change in a superconducting material as the detection mechanism: when a photon is absorbed in a narrow superconducting wire, a local hotspot is formed, increasing the superconducting current density in the surrounding areas. When the critical current density is reached, the film switches into a resistive state [17]. This concept was demonstrated with 0.2-µm NbN ultrathin (5-nm) films with relaxation times of around 100 ps [18]. An advantage of SNSPDs is that they operate at higher temperatures than TES, often near 4 K [9].

However, the absorption rate in SNSPDS are typically lower than for TES. To increase the optical coupling, thin NbN nanowires in meander structures, such as shown in Fig. 1, have been demonstrated to have higher detection efficiencies. A 3.3 µm × 3.0 µm device, with an optical cavity and AR coating to minimize reflections, was demonstrated with a detection efficiency of ~50% [8].

The detectors described above are illuminated from above the substrate, typically via an optical fiber. Integrating these sensors in photonic integrated circuits (PICs) may be the next step in achieving practical modules for experiments and devices in quantum optics, communications, and other related fields (see e.g., references in [19]). The efficiency of SNSPDs is improved by evanescent coupling by a waveguide integrated in the chip, as the wave may interact with the detector over a longer distance. For example, 91% chip detection efficiency has been demonstrated for SNSPD wires on top of a silicon waveguide [20], while on-chip measurement of entangled photon pairs were demonstrated in [19].

Similarly, 88% detection efficiency has been demonstrated for a PIC with three TES in series on top of a silica waveguide [21]. A challenge remains, however, in the fiber-to-waveguide coupling, where significant coupling losses may occur [20, 21], as discussed in more detail in the section "Interconnections, Packaging, and Integration."

B. Optically Controlled Superconducting Electronics

In a number of studies, optically controlled superconducting systems are described. Here, current pulses are generated by semiconductor photodiodes/photoconductors, connected to superconducting electronic circuits. These systems exploit macroscopic quantum phenomena, which emerge as a result of the behavior of Josephson junctions. Such systems have been proposed as a candidate for next-generation computing and communications systems, due to the high speed and low power consumption and are based on so-called rapid single flux quantum (RSFQ) circuits, where information "is stored in a superconducting loop as a flux quantum" [1]. Josephson junctions consist of an ultrathin insulating barrier between two superconducting sections. In the superconducting state, the current has the ability to tunnel through the junction, with no power loss. The superconducting current, J_s, is determined by the phase difference across the junction [22]:

$$J_s = J_c \sin(\theta) \quad (2)$$

By controlling the superconducting current with short pulses, the phase difference develops, leading to the formation of a

Downloaded from http://meridian.allenpress.com/jmep/article-pdf/12/4/189/2245811/imaps_485.pdf by guest on 31 October 2022

voltage across junction, which can be determined by the phase-voltage relation [22]:

$$U(t) = \frac{\hbar}{2e}\frac{\partial\theta}{\partial t} \tag{3}$$

The operation of Josephson junctions in RSFQ circuits is based on switching the phase of the junction by a current pulse.

As the phase difference after the pulse must be a multiple of 2π, the time integral of the voltage is quantized, given by fundamental physical constants:

$$\int U dt = \frac{\hbar}{2e} \cdot 2\pi \cdot n = \frac{h}{2e} n \tag{4}$$

where n is a quantum step number. $N = 1$ corresponds to a magnetic flux quantum, $\Phi_0 = h/2e$, transferred across the junction. A family of digital logic/memory based on this principle is described in [23].

Related, in metrology, Josephson junction arrays (JJAs) consisting of several 100s to 1,000s of Josephson junctions in series have been developed for voltage standard applications. The generation of quantum accurate direct current voltages by JJAs is today in use [24], based on biasing the Josephson junctions by microwave radiation, with commercial suppliers of these devices.

A method of generating arbitrary voltage waveforms by pulsed operation of JJAs was proposed [25]: a current pulse switches the phase of the junction by 2π. Thus, the time-averaged voltage over each Josephson junction is given by fundamental constants:

$$V = \frac{h}{2e} f \tag{5}$$

By modulating the frequency f of the input pulses, quantum accurate voltage waveforms can be produced. A combination of positive and negative pulses enables the generation of bipolar waveforms. Optical generation of the electrical pulses by a pair of photodiodes, rather than a direct electrical input, has several advantages, such as optical isolation from the pulse generator and possibility of adjusting the optical power by optical attenuators [26].

Also for RSFQ circuits, an optical input offers advantages over coaxial cables. As Josephson junction circuits are capable of high speeds, several 10s of GHz, an electrical input is a major obstacle for the realization of these devices. Although high-speed coaxial Cu cables have been demonstrated up to 10 Gbps, they have a high thermal load on the system [27]. Development of systems based on optical generation of electrical pulses is in part motivated by the high loss, dispersion, and high thermal load of high-speed electrical cables [4, 28].

In contrast, an optical input, with a cooled photodiode near the circuit, coupled to an external source via an optical fiber, has a low heat impact on the system, and is capable of high speeds, as the electromagnetic signals are immune to cross talk. However, there are several challenges that must be taken into account when designing an optical input at cryogenic temperatures.

A suitable high-speed photodetector with high performance at 4 K must be selected. The relevant properties of semiconductors at these low temperatures obviously change from room temperature, including an increase in the band gap, decrease in thermal conductivity, and risk of charge-trapping effects [29].

Photodiode may either be integrated on a substrate or be connected as an external module by wiring. Metal-semiconductor-metal (MSM) photodiodes may be integrated on substrates by lithography, while commercial diodes, such as PIN diodes, may be mounted on the superconducting chip by flip chip bonding or adhesive bonding.

In structure, MSM diodes are simple in structure and consist of interdigitated metal fingers on the top of a semiconducting substrate. As such, it can be processed in a few lithographic steps. One example of an integrated silicon MSM diode, with the diode close to Josephson junctions on a single substrate, is seen in Fig. 2.

In part, the area of the diode and the width of the fingers and spacing determine the response time of the diode. By reducing the finger length and spacing, the response time decreases [31]. Different types of high-speed photodiodes such as MSM diodes and PIN diodes have been shown to perform well at cryogenic temperatures. The development of optoelectronic interfaces for digital superconducting electronics until 2001 is described in detail in [32]: silicon MSM diodes emerged as the natural choice for Nb-based superconducting chips, as these chips are fabricated on silicon substrates. Integrated Si and GaAs MSM photodiodes and laser diodes at 77 K was studied in [33], for the feasibility of optical input/output to Josephson junction circuits. In another study [34], silicon, GaAs, and InGaAs PIN and MSM diodes, in addition to InGaAsP laser diodes, were tested at 4.2 K, with multimode optical fiber input/output. Furthermore, successful operation of a superconducting circuit with optical input/output was demonstrated. The silicon PIN diode experienced carrier freeze out at 4 K. In contrast, InGaAs PIN diodes operated well at 4.2 K and with increased speed.

In [28], a pulsed signal was delivered to an RSFQ circuit via a single-mode fiber to a 20 μm × 20 μm silicon MSM diode with finger width and spacing of 1 μm. At a repetition frequency of 20.6 GHz, the voltage readout confirmed correct operation.

A test of several photodiodes at 77 K showed that the responsivity of a silicon PIN diode was reduced by only 8%, while noise was reduced considerably [35]. Investigation of

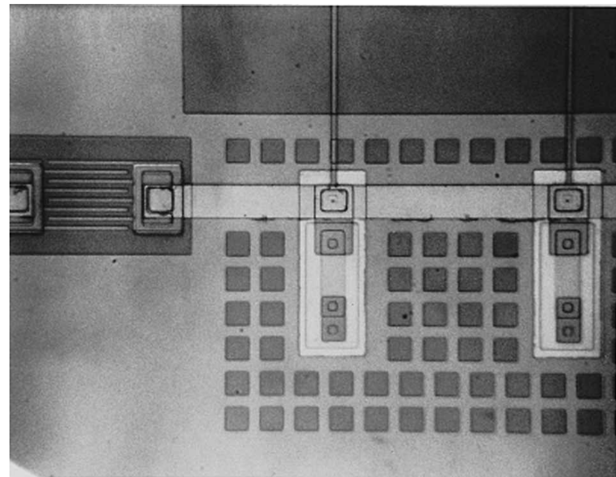

Fig. 2. A silicon MSM photodiode coupled with two Josephson junctions, used to generate single-flux pulses. Reproduced from [30].

Downloaded from http://meridian.allenpress.com/jmep/article-pdf/12/4/189/2245811/imaps_485.pdf by guest on 31 October 2022

a high-speed (>20 GHz) GaInAs/InP PIN diode showed that dark current was suppressed by a factor of 1,000 at cryogenic temperatures. In addition, no degradation of performance was found when cooled [36]. A commercial InGaAs MSM photodiode with an electrode gap width of 5 μm was demonstrated to drive JJA with 100 JJAs in series with a pulse repetition frequency of 50 MHz and pulse width of 100 fs [3]. A pulse width of 80 ps of the generated waveform was estimated inside the cryostat, indicating a 6.3 GHz operation possibility for the pulse trains. An optical input module based on an InGaAs substrate has been demonstrated at 4.2 K speeds reaching 1.5 GHz, with possibilities for speeds up to 10 GHz [37].

Uni-traveling carrier photodiodes (UTC-PDs) is a relatively new kind of photodiode, designed for high-speed and high-power output applications at long wavelengths, with a reported bandwidth as high as 310 GHz [38]. These have been used as the optoelectronic driver in superconducting systems, including 40 Gbps operation of single flux quantum (SFQ) circuits [4] and operation of JJA at 10 Gbps [39]. In these studies, modified commercial UTC-PD modules were connected to the superconducting circuits with coaxial cables.

Optics and Optical Coupling

Optoelectronic coupling involves guiding the electromagnetic wave from a source to the detector surface. Essentially, the energy in the wave can be described as a beam traveling from the source, exhibiting the usual phenomena of reflection and interference, before the energy is absorbed in the detector material. For high-speed semiconducting and superconducting devices, the desired low response time generally implies small detector areas, with typical diameters/widths ranging from 5 μm to 25 μm for surface-illuminated detectors.

The interface between the optical fiber and the cooled detectors, which are typically on the micrometer scale, requires a high alignment accuracy to ensure high coupling efficiency, whether the application is photon detection or for an optoelectronic driver.

Optical fibers/waveguides, mirrors, and lenses are the common components used to design coupling structures, and appear in the form of individual elements, or integrated structures on the device.

Single-mode fibers appear frequently in these types of high-speed optoelectronic circuits, as they provide a link between an external optical source and the cooled detector system. They are extremely useful due to their flexibility and ability to guide the optical pulses without loss. Optical fibers consist of a core and cladding of a flexible material, typically silica (SiO_2). The core has a slightly higher refractive index than the cladding, resulting in a guided mode within the fiber. Although most devices described here use single-mode fibers, multimode optical fibers are used in some applications: to achieve coupling of visible light from free space, a 50-μm multimode fiber terminated with a gradient index (GRIN) lens was coupled to an SNSPD in [40]. Compared with a coupling by a single-mode fiber, multimode fibers result in higher jitter in SNSPDs [40, 41], caused by modal dispersion of light pulses due to the difference in propagation velocities among modes.

Achieving efficient optical coupling is synonymous to limiting losses, which may be caused by several effects: when coupling to the detector area, unwanted losses occur due to reflections at interfaces and divergence of the optical beam, i.e., "reflections" are caused by the mismatch in refractive index between materials and can be calculated by the Fresnel equations [42]. The fiber-air interface is an obvious example: ~4% of the optical power is back-reflected.

Furthermore, in the coupling from the fiber to the detector, the electromagnetic wave is transmitted through several interfaces, where each interface leads to some back reflection. Two or more back-reflected waves may interfere destructively or constructively, influencing the total transmitted power. Thus, the total back-reflected power is dependent on the thickness and refractive indices of the layers, in addition to the wavelength.

To reduce the back reflection, an AR layer is often applied at the interfaces. In the case of transmission through an intermediate AR layer, interference between the back-reflected and incoming waves in the AR layer reduces the overall back-reflected power. When the thickness of the AR layer is a quarter wavelength ($d = (\lambda_0/4\pi n)$), the reflection coefficient, R, is [42]:

$$R = \frac{\left(n_0 n_2 - n_1^2\right)^2}{\left(n_0 n_2 + n_1^2\right)^2} \tag{6}$$

Choosing an AR layer with $n_1^2 = n_0 n_2$, in theory, the reflection is reduced to zero. For example, by applying an AR coating to the fiber end, the reflection can be reduced from 4% to 1% [5].

An additional cause of losses is due to divergence of the beam when propagating unguided in a material, such as in an air gap. To avoid losses due to this spreading of the beam, a minimum distance for free-space coupling can be calculated by considering the beam as a Gaussian function, which is a useful approximation for estimating the size of the wave. The Gaussian beam is characterized by a "beam waist," which is the radius of the beam where the amplitude is $1/e^2$ of the maximum amplitude. In free space, the beam waist, w, expands according to the equation:

$$\omega(z) = \omega_0 \left(1 + \frac{\lambda z}{\pi \omega_0}\right)^{\frac{1}{2}} \tag{7}$$

The optical path length between the layers can be determined by sweeping the wavelength and observing the reflected power. The spacing between fringes allows determining the fiber-detector distance and possible misalignment [5], as shown in Fig. 3.

In most cases, the active area of the detectors is produced parallel to a substrate. The optical beam must either couple directly, perpendicular to the substrate, or evanescently, with the wave traveling parallel to the substrate, using integrated waveguides.

In many cases, the optical coupling efficiency is optimized by orienting the optical fiber perpendicular to the detector surface, with a small gap in between.

The coupling efficiency in this kind of setup depends on the indices of refraction of the materials and the thicknesses in various layers; multiple reflections occur at the interfaces between materials with dissimilar refractive indices. Filling the volume between the fiber end and detector with a polymer eliminates the air gap, as in [6], shown schematically in Fig. 4,

Downloaded from http://meridian.allenpress.com/jmep/article-pdf/12/4/189/2245811/imaps_485.pdf by guest on 31 October 2022

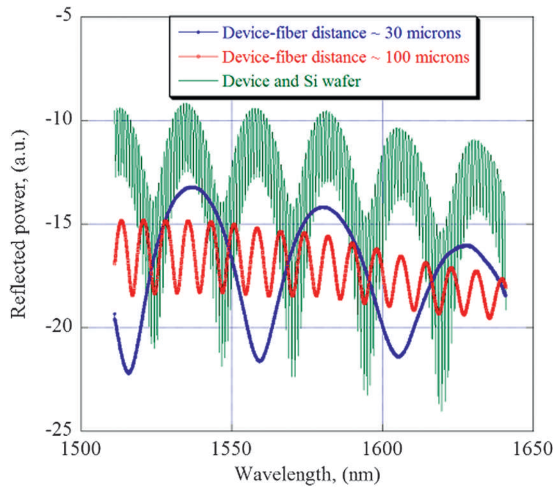

Fig. 3. Interference fringes used to find the fiber-chip distance and fiber-chip misalignment in [5].

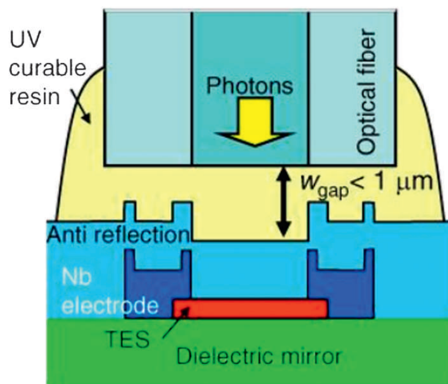

Fig. 4. Schematic diagram of an optical fiber bonded and coupled to a TES with a transparent resin. Reproduced from [6].

where the fiber was attached with UV-curable resin ($N = 1.56$) with thickness below 1 µm to the device. With this technique, 98% coupling efficiency to a TES was achieved.

In addition, direct coupling between optical fiber and detectors, bonded with adhesives, has been demonstrated at cryogenic temperatures for devices, such as photoconductive switches [43, 44], MSM photodiodes [37], and SNSPDs [8, 41].

As the use of adhesives is often a concern due to the high stress transfer to brittle materials, detector and risk of misalignment when cooled, support structures for the fiber, such as metallic housings, allow coupling to the fiber via an air gap (e.g., [45, 46]). These are discussed further in the section "Interconnections, Packaging, and Integration."

Other requirements, such as compactness and multiple fiber inputs, put constraints on the size and geometry of the packaged device. Orienting the optical fiber parallel to the substrate is a useful strategy to minimize the size. In addition, fabrication can be simplified by aligning the fibers in v-grooves patterned in a substrate or block of material, allowing high-density fiber optic input modules.

In the case of a top-/bottom-illuminated photodetector, this requires bending the light onto the active area. In [47], as shown in Fig. 5, with the fiber in a v-groove etched in the substrate, a CrAu-coated facet at a 55° incline in the substrate reflects the light to a PIN photodiode mounted on top of the substrate. This method showed "virtually no coupling loss."

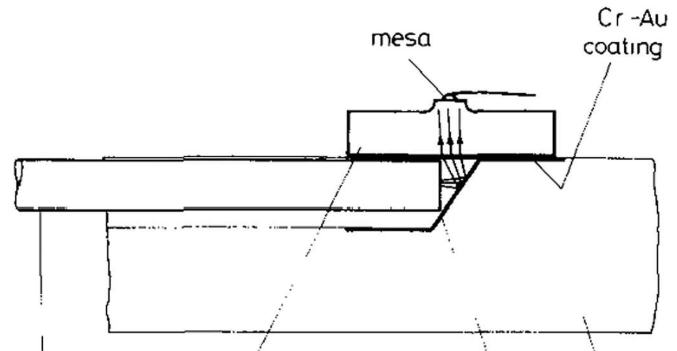

Fig. 5. Optical fiber coupled to photodiode via mirror etched in substrate. Reproduced from [47].

Alternatively, cleaving the fiber at a large angle, ideally the wave is reflected totally and exits the fiber at the side of the fiber. When the fiber is surrounded by air, the maximum cleaving angle is simply determined by Snell's law:

$$\theta T\ IR = \sin^{-1}\left(\frac{1}{1.46}\right) \approx 43^\circ \tag{8}$$

In [48], to achieve TIR (total internal reflection) at a 45° cleaving angle, a reflecting aluminum surface was deposited on a multimode optical fiber and glued to a receiver. Compared with direct coupling, additional coupling losses occurred, attributed mainly to wave spreading, surface roughness, reflectivity of the mirror, and other effects such as misalignment.

Coupling to a photodiode by 90° reflection can be avoided by using side-illuminated photodiodes, where the edges of the photodiode are angled and the incoming wave is refracted toward the active area [49].

In photonic chips, where optical fiber are connected to waveguides, rather than detectors, the waveguides often have dimensions down to some hundred nanometers. Thus, coupling tolerances may be even lower.

Coupling losses in an SNSPD integrated circuit occurred at the grating coupler from a fiber to a 750 nm × 110 nm waveguide [20].

A lensed fiber is used to couple to 500-nm-thick waveguides in an SNSPD photonic circuit [19]. Here, a loss of 3.7 dB occurred at the fiber-waveguide interface. However, the alignment of the fiber is not permanently fixed, but controlled by a precision stage.

Inverse tapering of waveguides was demonstrated in [50], to allow direct coupling between optical fibers and the waveguide with improved modal overlap, resulting in 1.9-dB loss after fixing the fiber module with adhesive.

Interconnections, Packaging, and Integration

As seen above, the optical coupling between an optical fiber and a detector requires considerations of the electromagnetic behavior and the geometry of the optical coupling. Possible designs will be limited by the available techniques for bonding

Downloaded from http://meridian.allenpress.com/imaps/article-pdf/12/4/189/2245811/imaps_485.pdf by guest on 31 October 2022

and packaging. Furthermore, requirements of size, materials, and cost will put constraints on the packaging scheme.

In optoelectronics, reducing the cost of fabrication and enabling high-volume production is a goal for next-generation devices [51], as accurate alignment and fixing of the fiber often is a time-consuming process. For devices operating in cryogenic environments, choosing suitable materials is especially important. In general, materials with low expansion should be chosen to reduce the influence of thermal deformations and stresses. Many standard commercial components may, therefore, be unsuited, as they do not fulfil these conditions. For example, certain plastic components, such as fiber holders may shrink considerably during the cooling, which may cause loss of optical coupling. In the following, some of the challenges and requirements of cryogenic optoelectronic devices is discussed, and some realized designs of the optical fiber-optical packaging is reviewed.

A. Optical/Electronic Integration and Interconnections

In some developments of superconducting devices, there is a trend toward developing integrated devices. Generally, this drive is motivated by the need to reduce influence of noise and propagation losses in high-speed electrical wiring. Additionally, external electrical wiring to the cooled system increases the thermal load on the system, increasing the power needed for cooling. Thus, certain developments are aimed at integration between optical and electronic components on a single-chip module or multichip module (MCM).

For example, for SNSPD arrays, as the potential counting rates is several gigahertz, replacing the conventional room-temperature readout with integrated SFQ electronics was proposed [52] and later demonstrated in [53, 54]. By wire bonding the detector directly to the SFQ circuit, as shown in Fig. 6, this is achieved.

For optically driven Josephson junction systems, the interface between the photodiode and the superconducting circuit poses a similar problem. In early developments, integrated MSM detectors fabricated on silicon substrates near to the Josephson junctions were demonstrated in a number of studies (e.g., [28, 30, 33]).

Later, in the development of JJA systems, commercial photodiode modules were used to drive the circuits: a photodiode was located outside the cryostat in [26], to drive a JJA via a 1-m coaxial cable, while a cooled MSM photodiode module was connected via coaxial cables to the JJA in [3].

In several studies, cooled UTC-PD modules were used: the UTC module was connected by a 23-cm Cu coaxial cable to the SFQ circuit in [4], reaching speeds of 40 Gbps. In another study of an integrated module for a high T_c superconducting sampler [52], the sampler chip is wire bonded to a photodiode chip, both located in the metal housing holding the two chips, as seen in Fig. 7.

Further improvements in high-speed performance can be achieved by developing such system into MCM with flip chip connections between the chips, further reducing the wire length. To allow multiple optical fiber inputs, an optical input module/carrier for an SFQ chip, with an InGaAs MSM diode fabricated on an InP substrate, has been designed [37], as seen in Fig. 8. The superconducting circuit is then flip chip bonded on top of the substrate. Alternatively, commercial photodiodes may be flip chip bonded to the superconducting chip, allowing integration of the diodes on the superconducting chip, as proposed in [34, 36].

The bonding and alignment of the optical fiber is a particular challenge in the device assembly, due to the high alignment accuracy needed. As the optical fiber often require adhesive bonding, or rely on complex housing structures for alignment, robustness and minimization of the device are often difficult to achieve. As the devices are cooled to cryogenic temperatures,

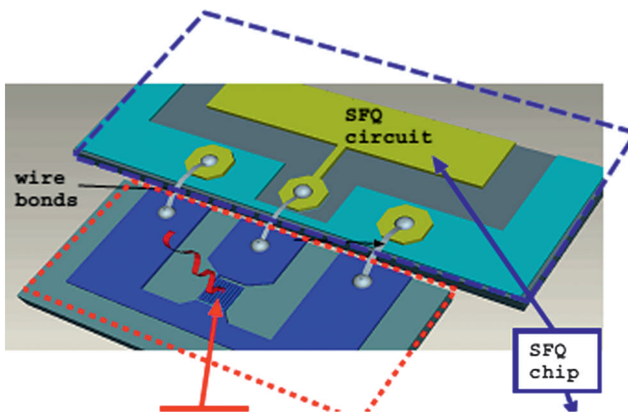

Fig. 6. SNSPD wire bonded to SFQ readout circuit. Reproduced from [54].

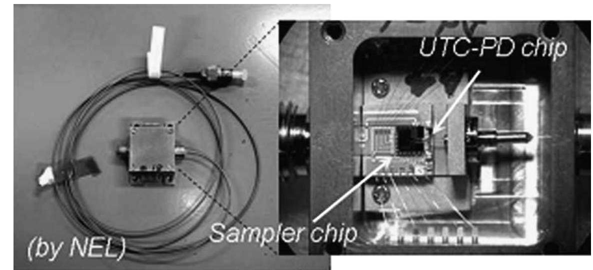

Fig. 7. Integrated UTC-PD/sampler module. Reproduced from [55].

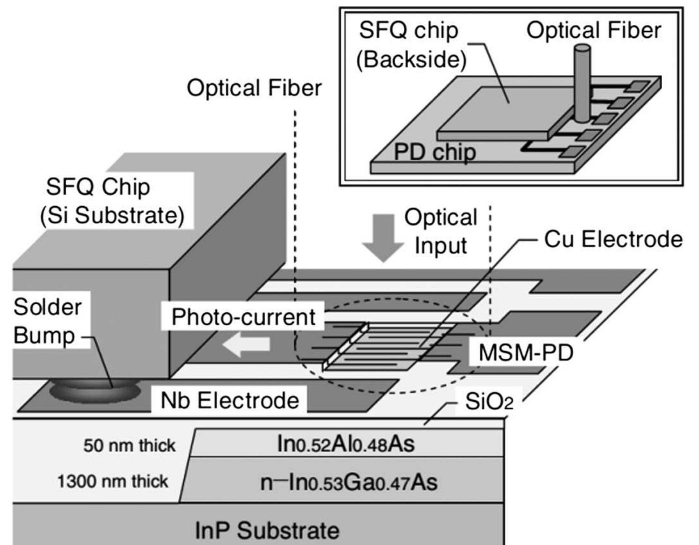

Fig. 8. Optical input module for superconducting chip. Reproduced from [56].

Downloaded from http://meridian.allenpress.com/jmep/article-pdf/12/4/189/2245811/imaps_485.pdf by guest on 31 October 2022

thermomechanical effects, shrinking of materials, may cause loss of optical connection. In particular, the high "coefficients of thermal expansion" (CTEs) of bonding materials, such as adhesives, are sources of high stress concentrations and deformation, since they are used to adhere to low-expansion substrate materials, such as silicon. Additional criteria for the package, such as multiple optical fiber input and size requirements put further constraints on the design of the optical input.

A traditionally packaged photodiode module, such as transistor outline cans and butterfly packages, fixes and aligns a single fiber to a metallic housing, with possibility of applying focusing with one or more ball lenses. Some limitations may follow from these designs. For example, alignment of multiple optical fibers and input may be difficult with this design, while development of MCMs, for example, might require planar/parallel fiber input to reduce size.

These challenges are shared with the recent developments in silicon photonics, which aims to replace electrical connections with high-speed optical connections. Thus, there is an effort to develop new technologies for optical fiber connections, in an effort to reduce cost and improve performance in terms of higher speed, multiple electrical input/outputs, reduced size and achieve high coupling efficiency [51].

For example, a quad flat no-lead package with a Si-Ge photodiode has been demonstrated, with the fiber directly coupled to photodiode by gluing with a UV-curable resin [57]. A self-aligning, passive alignment packaging of a vertical-cavity surface-emitting laser diode was demonstrated by etching a hole for the optical fiber through the silicon substrate [58]. The fiber, held in a ferrule, was aligned by a pick-and-place machine and glued to the substrate, achieving high alignment accuracy and reliable performance when thermally cycled between −40°C and −85°C.

In a number of papers, the techniques for fiber alignment and bonding for cryogenic applications are described. In the following, we review some practical solutions, which been demonstrated, differentiating between devices with single and multiple optical input.

B. Single Fiber Packaging

A substrate such as a Si wafer may contain one or more photodetectors, either bonded or produced directly by microfabrication. If only a single optical fiber input is required, a number of techniques for optical fiber assembly has been demonstrated.

Several demonstrations of cryogenic detectors apply direct, perpendicular bonding of the optical fiber using some adhesive. In [6], as shown previously in Fig. 4, a fiber with a mode field diameter of 4 μm is attached by filling the small (∼300-nm) gap with a UV-curable index resin, also acting as an AR layer. The misalignment in this setup was <1 μm, resulting in negligible coupling loss. Similarly, in [8], as shown in Fig. 9, a 15-μm core fiber was attached directly to a 50 μm × 50 μm NbN SNSPD grown on MgO substrate using a UV curing resin.

In [28], the optical fiber rests inside a glass capillary glued to the surface of a 50-μm-thick quartz spacer, which is subsequently glued to a 20 μm × 20 μm integrated MSM diode. The function of the quartz spacer is to protect the detector surface and to provide space for the wave to spread out to reduce local saturation effects in the detector.

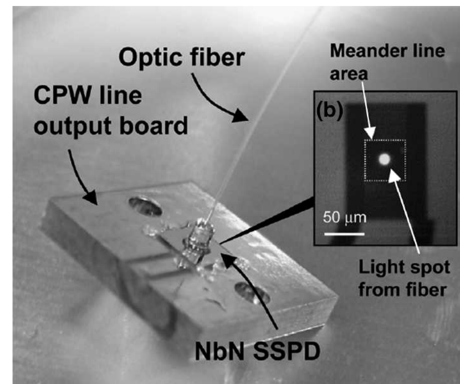

Fig. 9. Fiber glued to SNSPD detector. Reproduced from [8].

Similarly, a single-mode fiber was aligned and cemented 50 μm above a 10 μm × 10 μm GaAs photoconductive switch grown on a GaAs substrate [43]. The deformations during curing of the epoxy caused coupling loss of 35% of the amplitude of the sampled voltage pulse. In a similar setup, sampling measurements of a fiber-coupled photoconductive switch showed that mechanical displacement caused by the mismatches of CTEs during cooling affected the peak amplitude of the current [44].

As high-expansion adhesives, such as some UV-curable adhesives, are prone to stability problems, overcoating the adhesive with a silicone polymer or "cryo-type" epoxy may enhance robustness at cryogenic temperatures [59].

Alignment of the single-mode and multimode optical fibers to small-area (10 μm × 10 μm) SNSPD with a micromechanical photoresist ring is described in [41, 60]. The ring is aligned with marks in the substrate allowing better than 1-μm alignment of the fiber, as pictured in Fig. 10. Additional mechanical support of the optical fiber is provided with aluminum holders glued to the bottom copper flange. A maximum coupling efficiency of 33% is reached with this design: Significant misalignment due to contraction and tilting in the initial cooldown is suggested as the cause. Furthermore, for some detectors, microcracks in the fiber occurred, reducing the coupling efficiency to a very low value.

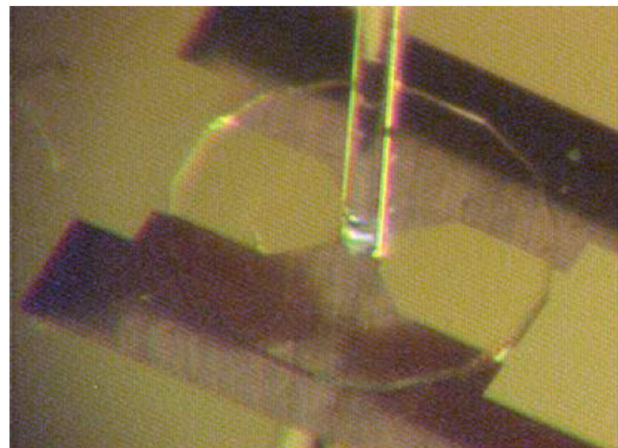

Fig. 10. Optical fiber aligned with micromechanical resist ring. Reproduced from [41].

Downloaded from http://meridian.allenpress.com/jmep/article-pdf/12/4/189/2245811/imaps_485.pdf by guest on 31 October 2022

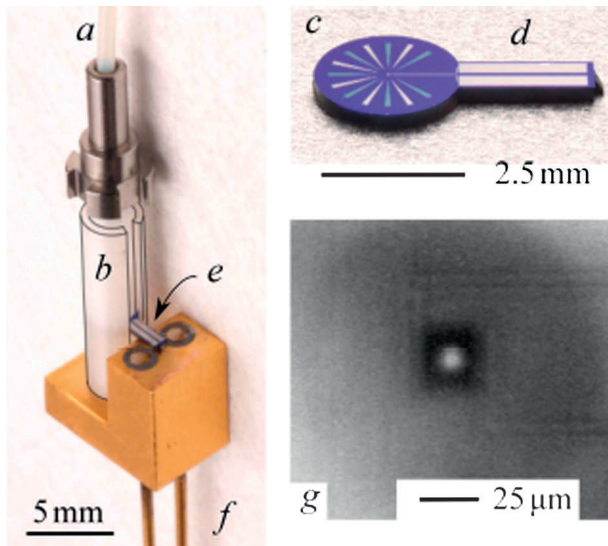

Fig. 11. "Self-aligned" SNSPD package, showing the (a) optical fiber, (b) alignment sleeve, (c-e) detector on machined silicon substrate, wirebonded to pins, and (g) an image of the optical beam. Reproduced from [61].

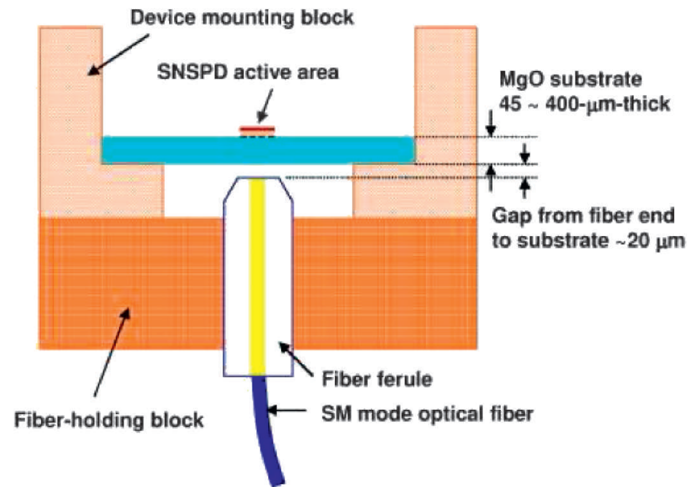

Fig. 12. Schematic diagram of SNSPD sensor housed in copper package. Reproduced from [62].

The use of adhesives is often seen as problematic in terms of reliability and stability, although systematic studies of these issues seems to be missing. Using structural components such as metal housings, ferrules, and alignment sleeves to hold the substrate and fiber, adhesive bonding of the fiber to the detector can be avoided.

In a "self-aligning" package described in [61], seen in Fig. 11, alignment is achieved by machining a substrate into a circular shape to fit a standard alignment sleeve holding an optical fiber inside a zirconia ferrule. This scheme resulted in an average alignment error of 3.1 µm, consistent with the undersizing of the machined substrate.

"Housing modules," where the substrate is bonded to machined metal blocks, provide a simple and reliable way to align single optical fibers to detectors. Two similar approaches for aligning the fiber-coupled SNSPDs are described in [46] and [62]. Here, optical fibers are glued inside ferrules, which are attached to the lid. By adjusting the position of the lid, the fiber is aligned by observing the optical beam. In [46], Invar 36 is chosen as the housing material due to its very low thermal expansion, with borosilicate as the ferrule material, while in [62], as seen in Fig. 12, the housing material is copper, with a zirconia ferrule. The SNSPD is illuminated through the sapphire substrate, achieving 98% coupling efficiency for a 45-µm substrate thickness.

To reduce the spot size at the detector, focusing lenses may be used. In [63], an SNSPD is illuminated through an MgO substrate. GRIN lenses were fused directly to the fiber end inside a ferrule to focus onto the detector.

A housing module, incorporating ball lenses and a spectral filter, was designed for fiber coupling to SNSPD arrays [64]. This allows an adjustable spot size, and multiple microlenses are etched into the Si substrate for coupling to an array of SNSPD detectors.

Another example of a detector module based on a metallic housing is found in [65]: Optical coupling to a UTC photodiode with a 30 μm^2 absorption area is achieved from an optical fiber via two aspheric lenses. The optical components and photodiode are welded to Invar holders in a Kovar package, showing good coupling stability when thermally cycled. To use such a module for driving superconducting electronics, a commercial module was modified, removing ferromagnetic material used to hold the lenses in [66]. Instead, the module was customized with a lensed fiber glued to a ferrule and brought close to the photodiode, as seen in Fig. 13.

Although packaging schemes using metallic housings may provide relatively simple and reliable alignment, the size and heat capacity may increase the cost of cooling. In addition, such solutions may be limited to a single fiber optical input.

Rather than permanently fixing and aligning the optical fiber, the beam may be directed to its target by precision stages, either coupled in free space by lenses from outside the cryostat through an optical window [30, 67] or aligned inside the cryostat by a micromechanical stage [19]. Having an optical window, however, increases the dark count rate due to radiation leakage [19].

For coupling a lensed fiber to a 500-nm-wide waveguide, the fiber is aligned by a slip-stick stage in the cryostat in [19]. Similarly, an optical fiber with fiber focuser was clamped

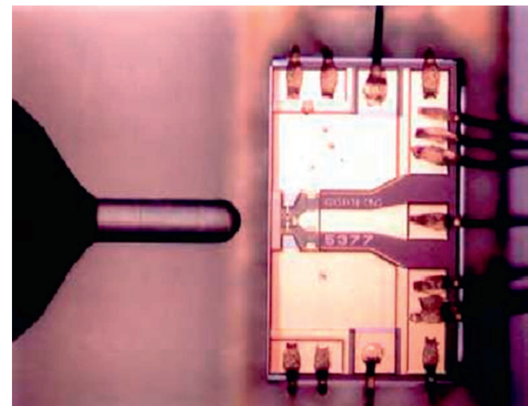

Fig. 13. Modified packaging of a UTC module: lensed optical fiber fixed with epoxy and coupled to side-illuminated photodiode. Reproduced from [66].

Downloaded from http://meridian.allenpress.com/jmep/article-pdf/12/4/189/2245811/imaps_485.pdf by guest on 31 October 2022

to a nanopositioner and coupled to a circular, 9-μm-diameter SNSPD [68].

The optical fibers are terminated by brass ferrules and focused by lenses in [45]: Motion control X-Y piezoelectric stages control the position of the ferrules to achieve alignment of the beam to photoconductive switches. This approach is chosen to avoid the destruction of the device and misalignment during curing and cooling of the glue.

As seen above, a ferrule is often used in the attachment of the fiber. Ceramic, glass, and metal ferrules are common materials.

For multimode fibers, focal ratio degradation may impact the output beam: Microbends in the fiber scatter the axial angles of incidence of guided rays [69]. Focal ray degradation due to thermal deformation at 77 K was studied in [70]. Results showed little effect on transmission for bare fibers, and only steel ferrules had an impact on focal ray degradation, while glass ferrules are better suited as the CTE matches that of the fiber.

C. Multiple Fiber Packaging

For some applications, multiple fiber input is needed. For example, a pair of balanced diodes are required for the generation of bipolar voltages in Josephson junction voltage standards.

In these cases, the schemes described above are less practical, as the vertical arrangement and bonding of optical fibers is space demanding; to save space and simplify alignment, planar structures, where one or more fibers is fixed parallel to the substrate, has advantages. A common technique to achieve this is to use so-called v-grooves in substrates: Multiple fibers may be passively aligned by simply press-bonding them into the grooves. An advantage of using v-groove holders is that the size of the device can be reduced. In addition, the assembly procedure can be simplified. However, the alignment of the fiber holder may be challenging and require specialized equipment.

V-grooves can be fabricated with high precision in a silicon substrate by wet etching [71] or sliced in glass components [72]. Studies of adhesively bonded optical fibers have shown that the placement and thickness of the adhesive influence the misalignment due thermal expansion of the epoxy [73], as the fiber may not properly touch the walls during the bonding of the fiber (Fig. 14).

To deal with the concern of the long-term improved resistance to creep and thermal cycling of adhesively bonded fibers,

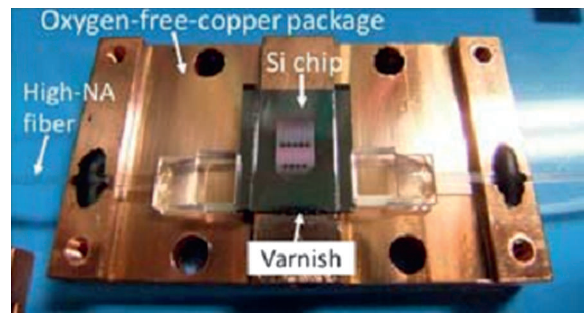

Fig. 15. Optical fibers coupled to silicon waveguides. Reproduced from [50].

solder bonding of optical fibers to silicon v-groove modules, by depositing multilayered coatings on the SiO_2 surface and optical fiber, has been demonstrated [74]. Anodic bonding of optical fibers to silicon v-grooves has also been demonstrated, requiring coating the fiber with high Na^+ glass [75].

Commercial v-groove modules have been used to couple optical fibers to waveguides in cryogenic photonic chips. As seen in Fig. 15, glass modules are aligned and bonded with a cryogenic type adhesive [50], showing good stability against thermal cycling. In a similar setup, for a TES photonic chip, misalignment was reported between the fiber holder and waveguide, when cooled [21].

V-groove holders may also be used to couple vertically onto a detector surface. This, however, may require an additional coupling step, with the bending of the wave. A patent of a cryogenic optical/electric interconnect module is described in [76], as shown in Fig. 16. The beam is reflected internally in the optical fiber onto the active area of a detector, with the optical fibers bonded by epoxy in v-grooves in a silicon fixture, which in turn is glued to a silicon fixture holding a photodiode array. Furthermore, these are bonded via an intermediate layer to a conductive base material. In this design, materials are chosen to match the CTE.

An example of the requirement of a dual optical input in metrology is mentioned in [15]: Two optical fibers, held in silicon v-groove modules, are coupled perpendicularly to a pair of TES detectors. This is achieved by gluing the v-groove holder to a copper angle bracket with an epoxy. Furthermore, the copper bracket was soldered to the substrate with an indium alloy, as shown in Fig. 17. Although the design theoretically

Downloaded from http://meridian.allenpress.com/jmep/article-pdf/12/4/189/2245811/imaps_485.pdf by guest on 31 October 2022

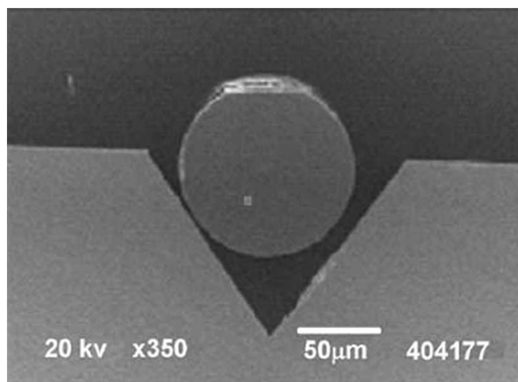

Fig. 14. Scanning electron microscopic image of optical fiber adhered with epoxy in silicon v-groove. Reproduced from [73].

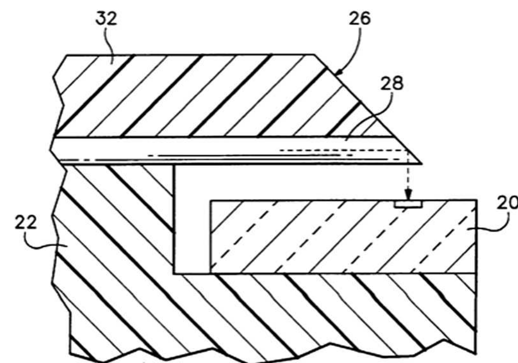

Fig. 16. Schematic diagram describing a cryogenic optical input module. Reproduced from [76].

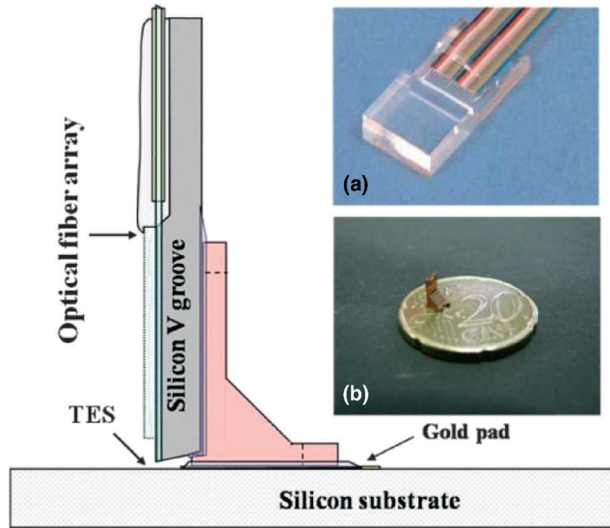

Fig. 17. Optical fibers coupled to TES detector, fixed in silicon v-groove holder. Reproduced from [15].

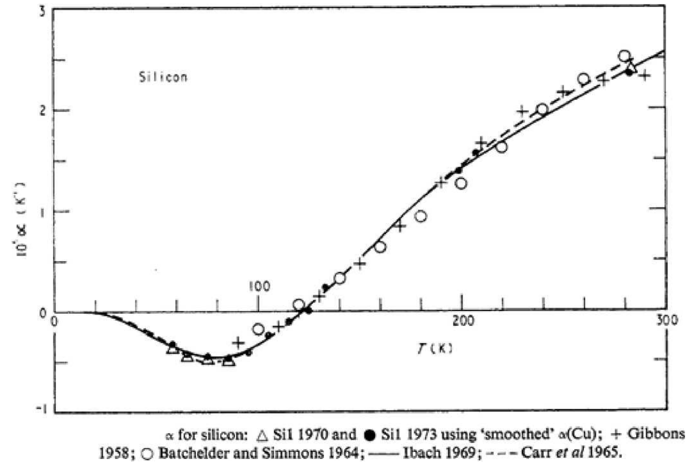

Fig. 18. Thermal expansion of silicon at low temperatures. Reproduced from [78].

allowed geometrical optical coupling by 100%, only 60% was reached due to defects in the bracket and the thickness of the solder.

Material Properties and Bonding at Cryogenic Temperatures

A. Low-Temperature Material Properties

As seen, fixing and aligning an optical fiber with high accuracy is a challenge in the design and assembly process, especially at cryogenic temperatures. Epoxies are commonly used for fiber bonding, while chips are often bonded in a flip chip process, with bonding materials, such as solders. The cooling of devices to cryogenic temperatures potentially puts large thermomechanical stresses on the package. Interfaces between adhesives and low expansion substrates/components are of particular concern, as they are locations for large stress concentrations. Selecting suitable adhesive or other bonding materials to minimize stress is an important part of the design process.

In microelectronic packaging, a main concern is often the shearing and peeling stresses at interfaces, as shown that can cause adhesive or cohesive failure, or cracking in brittle materials [77]. Thus, the design of the joint geometry should be made to minimize peel and tensile stresses as this reduces the chance of crack initiation at the interfaces. The strength and robustness to thermal cycling is a condition for the realization of these kinds of cryogenic devices. When cooled, stresses and deformations are induced in the materials due to differences in thermal expansion (contraction) of the components. Although optical components and substrates typically have low expansion, solders and adhesives commonly used for bonding have higher expansion.

The CTE, relates the change in length, dL, with a temperature change, dT:

$$\alpha = \frac{1}{L}\frac{dL}{dT} \tag{9}$$

As α is a temperature-dependent property, the total contraction ΔL is found by integration:

$$\Delta L = \int \alpha dT \tag{10}$$

In general, α increases with increasing temperatures and is reduced to 0 at absolute zero. For example, silicon, which is commonly used as the substrate material, has a low thermal expansion and, notably, a negative CTE from ~0 K to 120 K [78], as seen in Fig. 18. Negative thermal expansion is also found in other materials, such as silica [78] and borosilicate glass (Pyrex) [79].

B. Polymers, Such as Epoxies, Are Fundamentally Different from "Harder" Materials, Such as Metals

In metals, thermal expansion is due to the anharmonic binding potential, while in polymers the situation is more complicated: The binding forces in polymers are a combination of intra- and intermolecular forces, covalent bonds binding the atoms in a chain, and van der Waals forces acting between chains. The thermal expansion in polymers is a combination of negative and positive contributions [80], i.e., a small negative expansion due to transversal vibration of the chains, a small positive expansion due to covalent binding, and a large expansion due to interchain modes. At low temperatures, the expansion is dominated by van der Waals forces between the molecules, while at higher temperatures, stretching of the covalent bonds within the chains become dominant [81], leading to a temperature dependence of the CTE, which is characteristic for many polymers, as shown in Fig. 19.

At room temperature, the CTE for a pure epoxy depends on the type of resin and degree of crosslinking [81], but typically varies from 50 ppm to 80 ppm at room temperature, giving a total contraction from room temperature to 4 K of ~1%-1.5% [80, 82].

The thermally induced stresses will largely depend on the "elasticity" of the materials. The elasticity of a material describes its stiffness: The force required to deform an object:

$$E = \frac{tensile\ stress}{extensional\ strain} = \frac{\sigma}{\eth} \tag{11}$$

Downloaded from http://meridian.allenpress.com/jmep/article-pdf/12/4/189/2245811/imaps_485.pdf by guest on 31 October 2022

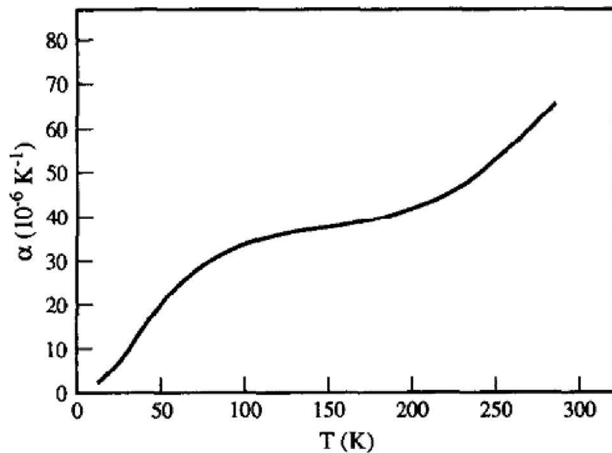

Fig. 19. Characteristic dependence of the CTE for polymers. Reproduced from [81].

For brittle materials, fracturing occurs at stresses higher than the yield strength, while ductile materials deform plastically before fracturing at the tensile strength. These properties too are temperature dependent. The elastic modulus and strength of materials generally increase at lower temperatures. Notably, polymers, such as epoxies, are brittle at low temperatures, while many solders and metals may remain relatively ductile. For many materials, however, the increase may be modest. For example, a 10% increase can be expected for some metallic alloys [83], while some solders may experience significant changes in strength and ductility at low temperatures [84].

Epoxies are characterized by a significant increase in both stiffness and strength when cooled: the increase in strength and elastic modulus of pure epoxy at lower temperatures is related to the shrinking, i.e., during cooling, the free space between molecules in the epoxy matrix disappears, leading to an increase in the molecular intermolecular forces [85]. Although epoxies may show some plasticity at room temperature, and increasingly near the glass transition temperature, they become increasingly brittle when cooled, as shown for a neat epoxy in Fig. 20. However, some epoxies may show a small amount of plastic behavior even at 4 K [82].

To reduce the thermal expansion, cryo-type epoxies are typically modified with low-expansion fillers. For example, modifying an epoxy with 4 wt.% SiO_2 nanoparticles may reduce the CTE from ~62 ppm to ~45 ppm at room temperature [87]. Likewise, 3 wt.% carbon black reduces the thermal expansion of the neat epoxy by 40% [86].

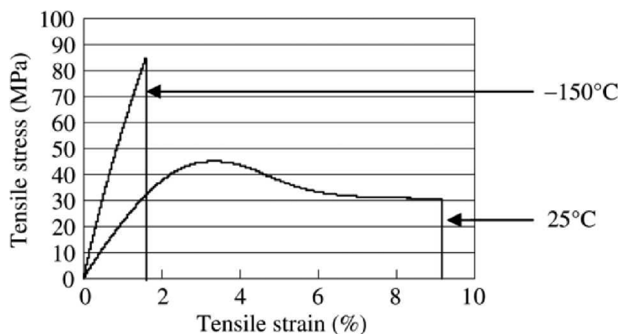

Fig. 20. Stress-strain curves of neat epoxy. Reproduced from [86].

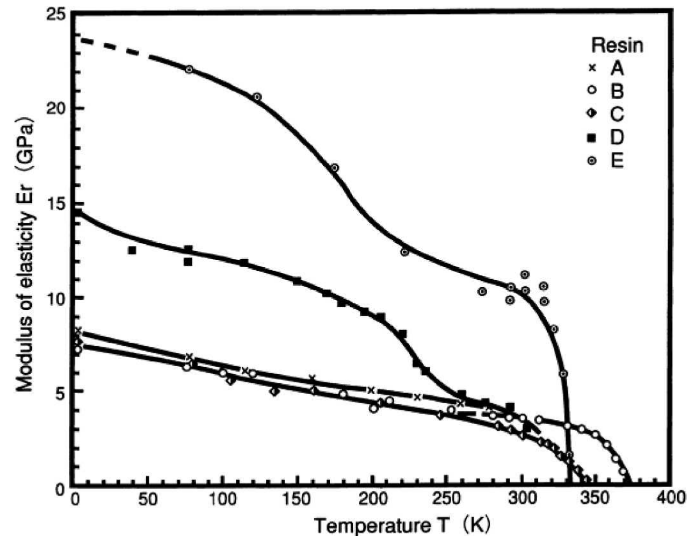

Fig. 21. Elastic modulus at low temperatures. A, B, and C are pure epoxies, while D and E are filled. Reproduced from [82].

However, the mechanical properties, such as the elastic modulus and strength, also change when fillers are added. In [82], mechanical properties of several types of epoxies were tested from T_g to 4 K, of which two of the epoxies had fillers.

The cost of reducing thermal expansion by fillers, however, is often an increase in elastic modulus and brittleness. There is a significant increase in the modulus when cooled from room temperature, and the filled epoxies showing a larger increase than the unfilled, as seen in Fig. 21. For all the samples, the maximum strain before fracture decreases steadily at lower temperatures.

The addition of nanosized filler particles to the epoxy resin may enhance the mechanical strength at cryogenic temperatures, due to an increase in interfacial adhesion between the resin and particles [87, 88]. For example, adding silica nanoparticles will increase both the tensile strength and elastic modulus at 77 K, while reducing the thermal expansion [87]. However, above an optimal weight percentage, the strength may decrease, for different reasons: For carbon-black-filled epoxies, it was observed that the tensile strength decreased at increasing concentrations [86]. It was speculated that the particles "prevented the shrinkage of the polymer networks, which interfered with the intermolecular forces at the cryogenic temperature."

A number of commercial epoxies are marketed as suitable for cryogenic environments. For example, Stycast 1266 and 2850FT are often referred to as "work horses" for low-temperature physics [89]. In [90], the mechanical properties of Stycast 1266, modified with quartz particles were studied: Adding silica fillers increased the elastic modulus while lowering the yield strength at cryogenic temperatures.

C. Bonding at Cryogenic Temperatures

The reliability and thermomechanical behavior of microelectronics packaging has been extensively studied, although there may be a less understanding of the reliability of cryogenic

Downloaded from http://meridian.allenpress.com/imep/article-pdf/12/4/189/2245811/imaps_485.pdf by guest on 31 October 2022

packaging. Some results of adhesively bonded optical components at cryogenic temperatures are discussed in the previous section, with some authors reporting issues with adhesively bonded components, although systematic reliability studies seem to be lacking.

Nevertheless, principles and results from packaging of "ordinary" electronics may be transferred to cold electronics. For example, in an adhesively bonded die to substrate, the difference in expansion between die and substrate lead to bending, with resulting peel and shear stresses. Increasing the thickness of the adhesive leads to lower shear and peel stresses at elevated chip temperatures. As a thicker adhesive layer leads to a decrease in the heat conductivity, an optimum adhesive thickness can be found [91].

On the other hand, thick adhesive layers can lead to unacceptable stress transfer to brittle materials such as a silicon substrate, leading to fracturing. The bonding between two silicon wafers with epoxy for a cryogenic application is discussed in [90]: Epoxy with high elastic modulus caused cracking in the silicon wafers for thick adhesive layers (>500 μm) when thermally cycled to 77 K.

Similarly, in [92], it was shown that thicker adhesive layers led to lower shear strength of single-lap joints with metal adherents. The explanation suggested was that the "plastic zone around the crack tip was not confined by the adherents," giving a lower fracture toughness. In addition, the higher thermal stresses in the adhesive due to CTE mismatches would give lower shear strength.

In addition to the thickness, the elastic modulus of the adhesive is an important property to consider. A study of a laser-fiber assembly found that "maximum von Mises stress varied inversely with the thickness and proportionally with the modulus" [93].

To reduce stress transfer to brittle substrates, a compliant epoxy, meaning one with low elastic modulus should be used. This selection criteria was used to select an adhesive for bonding a charge coupled device intended for a space telescope [94] and for bonding cryogenic optics [95], and to select an epoxy used for bonding microwave-integrated circuits operating at cryogenic temperature [96].

As seen previously, the tensile strength of epoxy increases at low temperatures. Adhesive double lap joints at low temperatures (−150°C) were studied in [97]. Tensile tests showed that joint strength increases at −150°C, while failure was caused by the crack initiating and propagating from the adherent interface.

The significant thermal residual stresses due to the cooling may reduce the bonding strength: The shear strength in an adhesively bonded (carbon-black-filled epoxy) double joint was reduced at cryogenic temperatures compared with room temperature [86], due to the thermal residual strains at this temperature. After thermal cycling of this epoxy to −150°C, the shear strength was reduced, depending on the filler weight percentage [86], as shown in Fig. 22.

Such "fatigue failure" may be responsible for 90% of all structural and electrical failures [98] in microelectronic packaging. The effect of cryogenic temperature cycling of some adhesives was tested in [89]: a thin layer of epoxy between two glass plates was subjected to thermal cycling to 77 K, and then the bond strength was tested in a simple test by applying a torque. Although some adhesives released at a high torque, others fractured internally in the cooling, as opposed to debonding.

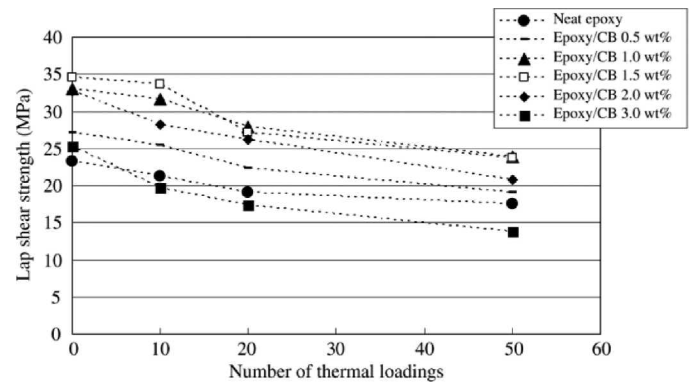

Fig. 22. Lap shear strength in an epoxy-bonded double lap joint after several thermal loadings. Reproduced from [86].

Thermal fatigue in epoxies is caused by crack growth. At existing, small flaws in the material, such as a scratch, there will be a local stress concentration from which cracks grow. The ability to withstand fractures due to preexisting cracks is measured by the "fracture toughness," K, with the unit $Pa\sqrt{m}$. The fracture toughness and creep deformation in epoxies at cryogenic temperatures were studied in [82], finding that for decreasing flaw sizes, the strength of specimens level of to that of plain specimens. The fracture toughness of four resins at low temperatures is shown in Fig. 23 [82]. While decreasing temperature, the fracture toughness reaches a maximum ~80 K, and then decreases at lower temperatures, reaching room-temperature values.

Modifying the epoxy influences the fracture toughness: Epoxies filled with nanoclay and carbon-black-filled epoxies increased the fracture toughness at room temperature. However, at cryogenic temperature, the fillers reduces the fracture toughness and there was a decrease compared with the pure epoxy at cryogenic temperatures, from which it was concluded that "the intermolecular forces between polymer networks of the epoxy were much dominant than the toughening effect of the mixed nanoparticles at the cryogenic temperature" [99].

The curing schedule of the adhesive is important for good bonding. A high degree of curing, achieved by curing at higher temperatures, leads to a higher degree of crosslinking, which maximizes glass transition temperature and strength, while minimizing CTE [100]. However, a high curing temperature leads to higher residual strains when cooled. A study of a single lap adhesive showed that a high degree of curing increased the bonding strength at both cryogenic and room

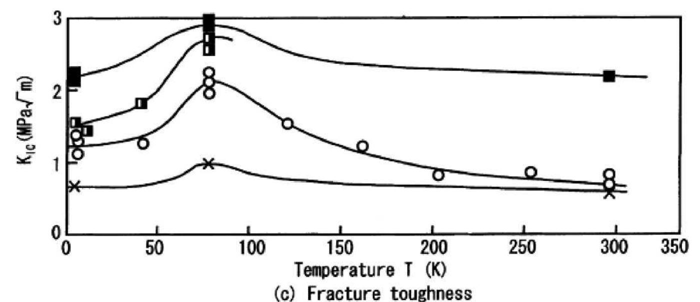

Fig. 23. The fracture toughness of three neat epoxies and a filled (squares) epoxy. Reproduced from [82].

Downloaded from http://meridian.allenpress.com/jmep/article-pdf/12/4/189/2245811/imaps_485.pdf by guest on 31 October 2022

temperatures [101]. Furthermore, "smart cure cycles," consisting of "gradual heating, rapid cooling, and reheating steps" could be used to minimize thermal residual stress.

In single-chip module or MCM, such as that seen in Fig. 8, the chip is mounted on a substrate. In flip chip bonding, metal bonds are formed between the backside of chip and the substrate with matching bond pads, providing both mechanical attachment and interconnections. As such connections have lower cross talk than wire bonds, they are commonly used in high-speed circuits. Solders are commonly used for optoelectronic chip attachment, such as photodiodes, due to their self-aligning ability. When melted, the surface tension in the solder bumps will act to minimize the surface, thereby aligning the chip with 1 μm precision with respect to the bond pads [102].

When choosing a solder material, several properties must be considered, such as melting temperature, Young's modulus, CTE, Poisson ratio, fatigue behavior, and creep rate [103]. A distinction can be made between "soft" solders, such as PbSn, InSn, and InPb, which are characterized by low melting temperature, increase in strength, and decrease in ductility at low temperature, and "hard" solders, such as AuSn, AuGe and AuSi, which do not undergo stress relaxation [104] (and references therein). A study on some Sn-based solders at cryogenic temperature found that the tensile strength increased, and then decreased when the temperature decreased [84]. Furthermore, tensile testing showed that fracturing was ductile at higher temperature, but brittle fracturing occurred at low temperature.

In chip attachment for superconducting modules, some studies on the mechanical reliability are reported, primarily using so-called soft solders, sometimes with an adhesive underfill: PbSn bumps, formed by a wire bonder, were demonstrated as connections between a superconducting Si chip and Al_2O_3 substrate, surviving several thermal cyclings to 4 K [105]. Furthermore, it was shown that the shear strength depended on the pad metallization, with Nb/Pd pads performing better than Nb/Au.

InSn solder bumps seem to be a commonly used solder material in many superconducting applications, as seen in several reports: for example, Josephson chips bonded directly to flexible carriers with InSn solder eliminated previous problems with mechanically worn spring-finger contacts, as reported in [106]. Additionally, InSn bumps are used in several superconducting MCMs, such as for bonding SFQ chips on a carrier (see e.g., [4, 66]).

A flip chip process for forming solder bumps and attaching superconducting dice was described in [107], with the bonding process shown in Fig. 24. InSn solder bumps are first formed on the pads, which have a Ti/Pd/Au layer onto Nb by immersion in liquid solder. The solder bumps, which become

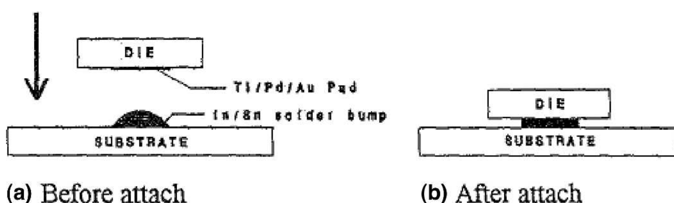

Fig. 24. Schematic diagram showing the principle behind flip chip attachment of die to substrate with In/Sn reflow soldering: a solder bump is deposited on the substrate, and the die is bonded by aligning the die and heating to the melting point of the solder. Reproduced from [107].

superconducting <10 K, adhere only to the wettable pads, forming bumps with an average height ~12 μm. After thermal cycling, the bonding had low failure rate (300 ppm), high reliability, and acceptable thermal resistance.

Thirty micrometer InSn bumps formed by immersion was used to bond superconducting chips in [108], transferring SFQ pulses at over 10 Gbps. Another group, however, in [109], reported that this technique did not provide sufficient mechanical stability for a superconducting MCM module, and the bonding was enhanced with a nonconducting adhesive, showing stability against thermal cycling. Expanding on this, the thermal conductivity of the adhesive can be increased using thermally conductive fillers. Single-walled carbon nanotubes are used as fillers in [110] to enhance the thermal conductivity of a commercial epoxy "without compromising its electrical properties." In [111], thermal simulations showed that this adhesive, when used as underfill for an InSn electrically bonded superconducting MCM, the temperature difference between the chip and substrate reduced the temperature difference by 86%.

Chip attachment by indium in cryogenic environments has been studied, due to its low melting point and high ductility, i.e., the reliability of indium joints for chip attachment of SiGe modules for Martian and lunar exploration were studied in [112], finding satisfying lifetime for such missions. Electroplated indium bumps were produced and their high-speed characteristics tested up to 100 GHz in [113], for a flip chip bonded chip, in combination with an adhesive, surviving over 100 thermocycles.

Summary and Conclusions

Fiber-coupled devices operating at cryogenic temperatures are being developed, with applications in several technologies. Superconducting optical detectors have applications in quantum communications and research, while an optical signal input is often desirable for superconducting electronics. In both cases, the design and packaging of the fiber-to-detector coupling may be a challenge.

Ideally, the manufacturing of these devices should yield cheap, robust devices with small size, with possibility of integration between optical and electronic components. However, compromises must often be made to obtain a practical device. For example, direct bonding of optical fibers with transparent adhesives might enable low-cost, simple assembly, although the long-term stability of adhesive bonds is typically lower than other methods.

Eliminating the use of such adhesive bonds is useful for reducing the thermal residual stresses. However, this requires more complex supporting structures for the optical fiber, typically using housing components, increasing the size of the package.

Another strategy for reducing the size of the package is to develop planar structures, although this strategy might require a more complicated optical coupling, resulting in more manufacturing steps and lower tolerances for alignment accuracy. Few demonstrations of such packages have been demonstrated, except for some integrated optical circuits with the fibers coupled to waveguides.

Developing suitable adhesive and metallic bonding techniques is critical for enabling a reliable and robust package. The increase in stiffness in all materials at cryogenic temperatures means that

Downloaded from http://meridian.allenpress.com/jmep/article-pdf/12/4/189/2245811/imaps_485.pdf by guest on 31 October 2022

the bonding material must be chosen with care. Several possible failure mechanisms are plausible at cryogenic temperatures, such as cracking in brittle substrates or debonding at material interfaces. Thus, generally, bonding materials of low thermal expansion with high compliance should be chosen. In addition, the joint geometry and layer thicknesses should be optimized.

Further progress in these technologies may lead to closer integration between the optical input and electronic circuitry. In addition, standardization of coupling techniques and the development specialized optical fiber components would be welcomed, opening up for the commercialization of such devices.

Acknowledgments

This work was partly carried out with funding by the European Union within the European Metrology Research Programme (EMRP) JRP SIB59 Q-WAVE. The EMRP is jointly funded by the EMRP participating countries within the European Association of National Metrology Institutes and the European Union. In addition, the work was also partly funded by scholarship provided by the Norwegian Ministry of Education and Research (KD-stipend).

References

[1] H. Hayakawa, N. Yoshikawa, S. Yorozu, and A. Fujimaki, “Superconducting digital electronics,” *Proceedings of the IEEE*, Vol. 92, No. 10, pp. 1549-1563, 2004.

[2] R.P. Mirin, S.W. Nam, and M.A. Itzler, “Single-photon and photon-number-resolving detectors,” *IEEE Photonics Journal*, Vol. 4, No. 2, pp. 629-632, 2012.

[3] C. Urano, N. Kaneko, M. Maezawa, S. Gorwadkar, T. Itatani, H. Saitou, J. Maeda, and S. Kiryu, “Operation of Josephson junctions with current pulses generated by triggering a cold photo detector with an optical comb,” *IEEE Transactions on Applied Superconductivity*, Vol. 17, No. 2, pp. 870-873, 2007.

[4] Y. Hashimoto, H. Suzuki, M. Maruyama, K. Fujiwara, and M. Hidaka, “40 Gbit/s operation of superconductive single flux quantum digital integrated circuit with optical data input,” *Electronics Letters*, Vol. 45, No. 1, pp. 87-88, 2009.

[5] A.E. Lita, A.J. Miller, and S.W. Nam, “Counting near-infrared single-photons with 95% efficiency,” *Optics Express*, Vol. 16, No. 5, pp. 3032-3040, 2008.

[6] D. Fukuda, G. Fujii, T. Numata, K. Amemiya, A. Yoshizawa, H. Tsuchida, H. Fujino, H. Ishii, T. Itatani, S. Inoue, and T. Zama, “Titanium-based transition-edge photon number resolving detector with 98% detection efficiency with index-matched small-gap fiber coupling,” *Optics Express*, Vol. 19, No. 2, pp. 870-875, 2011.

[7] N.A. Tomlin, J.H. Lehman, and S. Nam, “Towards a fiber-coupled picowatt cryogenic radiometer,” *Optics Letters*, Vol. 37, No. 12, pp. 2346-2348, 2012.

[8] S. Miki, M. Fujiwara, M. Sasaki, and Z. Wang, “NbN superconducting single-photon detectors prepared on single-crystal MgO substrates,” *IEEE Transactions on Applied Superconductivity*, Vol. 17, No. 2, pp. 285-288, 2007.

[9] M. Grein, E. Dauler, A. Kerman, M. Willis, B. Romkey, B. Robinson, D. Murphy, and D. Boroson, “A superconducting photon-counting receiver for optical communication from the Moon.” SPIE Newsroom, July 2015; doi: 10.1117/2.1201506.005932.

[10] C.M. Natarajan, M.G. Tanner, and R.H. Hadfield, “Superconducting nanowire single-photon detectors: physics and applications,” *Superconductor Science and Technology*, Vol. 25, No. 6, 063001, 2012.

[11] K.D. Irwin and G.C. Hilton, “Transition-edge sensors,” in *Cryogenic Particle Detection*, C. Enss, ed., Springer, Berlin Heidelberg, pp. 63-150, 2005.

[12] K.D. Irwin, “An application of electrothermal feedback for high-resolution cryogenic particle detection,” *Applied Physics Letters*, Vol. 66, No. 15, pp. 1998-2000, 1995.

[13] M.D. Eisaman, J. Fan, A. Migdall, and S.V. Polyakov, “Invited review article: single-photon sources and detectors,” *The Review of Scientific Instruments*, Vol. 82, No. 7, p. 071101 2011.

[14] A.J. Miller and A.V. Sergienko, “Demonstration of a low-noise near-infrared photon counter with multiphoton discrimination,” *Applied Physics Letters*, Vol. 83, No. 4, pp. 791-793, 2003.

[15] L. Lolli, E. Taralli, C. Portesi, D. Alberto, M. Rajteri, and E. Monticone, “Ti/Au transition-edge sensors coupled to single mode optical fibers aligned by Si V-groove,” *IEEE Transactions on Applied Superconductivity*, Vol. 21, No. 3, pp. 215-218, 2011.

[16] C. Portesi, E. Taralli, L. Lolli, M. Rajteri, and E. Monticone, “Fabrication and characterization of fast TESs with small area for single photon counting,” *IEEE Transactions on Applied Superconductivity*, Vol. 25, No. 3, pp.1-4, 2015.

[17] A.D. Semenov, G.N. Gol’tsman, and A.A. Korneev, “Quantum detection by current carrying superconducting film,” *Physica C: Superconductivity*, Vol. 351, No. 4, pp. 349-356, 2001.

[18] G.N. Gol’tsman, A.A. Korneev, and A.D. Semenov, “Picosecond superconducting single-photon optical detector,” *Applied Physics Letters*, Vol. 79, No. 6, pp. 705-707, 2001.

[19] F. Najafi, J. Mower, N. Harris, F. Bellei, A. Dane, C. Lee, P. Kharel, F. Marsili, S. Assefa, K.K. Berggren, and D. Englund, “On-chip detection of non-classical light by scalable integration of single-photon detectors,” *Nature Communications*, Vol. 6, p. 6, 2015.

[20] W.H.P. Pernice, C. Schuck, O. Minaeva, M. Li, G.N. Goltsman, A.V. Sergienko, and H.X. Tang, “High-speed and high-efficiency travelling wave single-photon detectors embedded in nanophotonic circuits,” *Nature Communications*, Vol. 3, p. 5873, 2012.

[21] B. Calkins, P.L. Mennea, A.E. Lita, B.J. Metcalf, W.S. Kolthammer, A. Lamas-Linares, J.B. Spring, P.C. Humphreys, R.P. Mirin, J.C. Gates, P.G. Smith, I.A. Walmsley, T. Gerrits, and S.W. Nam, “High quantum-efficiency photon-number-resolving detector for photon icon-chip information processing,” *Optics Express*, Vol. 21, No. 19, pp. 22657-22670, 2013.

[22] A. Barone and G. Paternò, *Physics and Applications of the Josephson Effect*, Wiley, New York, 1982.

[23] K.K. Likharev and V.K. Semenov, “RSFQ logic/memory family: a new Josephson-junction technology for sub-terahertz-clock-frequency digital systems,” *IEEE Transactions on Applied Superconductivity*, Vol. 1, No. 1, pp. 3-28, 1991.

[24] C.A. Hamilton, R.L. Kautz, R.L. Steiner, and F.L. Lloyd, “A practical Josephson voltage standard at 1 V,” *IEEE Electron Device Letters*, Vol. 6, No. 12, pp. 623-625, 1985.

[25] S.P. Benz and C.A. Hamilton, “A pulse-driven programmable Josephson voltage standard,” *Applied Physics Letters*, Vol. 68, No. 22, pp. 3171-3173, 1996.

[26] J.M. Williams, T.J.B.M. Janssen, L. Palafox, D.A. Humphreys, R. Behr, J. Kohlmann, and F. Müller, “The simulation and measurement of the response of Josephson junctions to optoelectronically generated short pulses,” *Superconductor Science and Technology*, Vol. 17, No. 6, pp. 815-818, 2004.

[27] Y. Hashimoto, S. Yorozu, T. Miyazaki, Y. Kameda, H. Suzuki, and N. Yoshikawa, “Implementation and experimental evaluation of a cryocooled system prototype for high-throughput SFQ digital applications,” *IEEE Transactions on Applied Superconductivity*, Vol. 17, No. 2, pp. 546-551, 2007.

[28] J.F. Bulzacchelli, L. Hae-Seung, S. Alexandrou, J.A. Misewich, M.B. Ketchen, “Optoelectronic clocking system for testing RSFQ circuits up to 20 GHz,” *IEEE Transactions on Applied Superconductivity*, Vol. 7, No. 2, pp. 3301-3306, 1997.

[29] A.K. Jonscher, “Semiconductors at cryogenic temperatures,” *Proceedings of the IEEE*, Vol. 52, No. 10, pp. 1092-1104, 1964.

[30] C.C. Wang, M. Currie, D. Jacobs-Perkins, M.J. Feldman, R. Sobolewski, and T.Y. Hsiang, “Optoelectronic generation and detection of single-flux-quantum pulses,” *Applied Physics Letters*, Vol. 66, No. 24, pp. 3325-3327, 1995.

[31] S.Y. Chou and M.Y. Liu, “Nanoscale tera-hertz metal-semiconductor-metal photodetectors,” *IEEE Journal of Quantum Electronics*, Vol. 28, No. 10, pp. 2358-2368, 1992.

[32] R. Sobolewski, “Ultrafast optoelectronic interface for digital superconducting electronics,” *Superconductor Science and Technology*, Vol. 14, No. 12, pp. 994-1000, 2001.

[33] B. Van Zeghbroeck, “Optical data communication between Josephson-junction circuits and room-temperature electronics,” *IEEE Transactions on Applied Superconductivity*, Vol. 3, No. 1, pp. 2881-2884, 1993.

Downloaded from http://meridian.allenpress.com/jmep/article-pdf/12/4/189/2245811/imaps_485.pdf by guest on 31 October 2022

[34] L.A Bunz, E.K. Track, S.V. Rylov, F.-Y. Perng, and J.D. Morse, "Fiber optic input and output for superconducting circuits," Paper presented at the Conference on Optics, Electro-optics, and Laser Applications in Science and Engineering (OE/LASE '94), 1994.

[35] D.V. Camin and V. Grassi, "Cryogenic behavior of optoelectronic devices for the transmission of analog signals via fiber optics," *IEEE Transactions on Nuclear Science*, Vol. 53, No. 6, pp. 3929-3933, 2006.

[36] Y.M. Zhang, V. Borzenets, N. Dubash, T. Reynolds, Y.G. Wey, and J. Bowers, "Cryogenic performance of a high-speed GaInAs/InP p-i-n photodiode," *Journal of Lightwave Technology*, Vol. 15, No. 3, pp. 529-533, 1997.

[37] H. Terai, S. Shinada, K. Makise, Z. Wang, and N. Wada, "An optical input module with superconducting single-flux-quantum circuit operating at 1550 nm," *IEEE Transactions on Applied Superconductivity*, Vol. 21, No. 3, pp. 896-899, 2011.

[38] H. Ito, T. Furuta, S. Kodama, and T. Ishibashi, "InP/lnGaAs uni-travelling-carrier photodiode with 310GHz bandwidth," *Electronics Letters*, Vol. 36, No. 21, pp. 1809-1810, 2000.

[39] C. Urano, M. Maruyama, N.-H. Kaneko, H. Yamamori, A. Shoji, M. Maezawa, Y. Hashimoto, H. Suzuki, S. Nagasawa, and T. Satoh, "Operation of a Josephson arbitrary waveform synthesizer with optical data input," *Superconductor Science and Technology*, Vol. 22, No. 11, 114012, 2009.

[40] D.K. Liu, T. Yamashita, L. You, Z. Wang, and H. Terai, "Multimode fiber-coupled superconducting nanowire single-photon detector with 70% system efficiency at visible wavelength," *Optics Express*, Vol. 22, No. 18, pp. 21167-21174, 2014.

[41] W. Slysz, M. Wegrzecki, J. Bar, P. Grabiec, M. Gorska, E. Rieger, S. Dorenbos, V. Zwiller, I. Milostnaya, O. Minaeva, A. Antipov, O. Okunev, A. Korneev, K. Smirnov, B. Voronov, N. Kaurova, G.N. Gol'tsman, J. Kitaygorsky, D. Pan, A. Pearlman, A. Cross, I. Komissarov, and R. Sobolewski, "Fiber-coupled NbN superconducting single-photon detectors for quantum correlation measurements," *Proceedings of SPIE*, Vol. 6583, pp. 65830J-1-65830J-11, 2007.

[42] O. Solgaard, *Photonic Microsystems: Micro and Nanotechnology Applied to Optical Devices and Systems*, Springer, Boston, MA, 2009.

[43] S. Verghese, N. Zamdmer, Q. Hu, and A. Förster, "Cryogenic picosecond sampling using fiber-coupled photoconductive switches," *Applied Physics Letters*, Vol. 70, No. 20, pp. 2644-2646, 1997.

[44] M. Griebel, J.H. Smet, J. Kuhl, K. von Klitzing, D.C. Driscoll, C. Kadow, and A.C. Gossard, "Picosecond sampling with fiber-illuminated ErAs: GaAs photoconductive switches in a strong magnetic field and a cryogenic environment," *Applied Physics Letters*, Vol. 82, No. 19, pp. 3179-3181, 2003.

[45] C.D. Wood, D. Mistry, L.H. Li, J.E. Cunningham, E.H. Linfield, and A.G. Davies, "On-chip THz generation and detection at milli-Kelvin temperatures for the study of ultrafast phenomena in confined semiconductor systems," Proceedings of the 2012 37th International Conference on Infrared, Millimeter, and Terahertz Waves (IRMMW-THz), pp. 1-3, Wollongong, New South Wales, 23-28 September, 2012.

[46] J.L.F.X. Orgiazzi and A.H. Majedi, "Robust packaging technique and characterization of fiber-pigtailed superconducting NbN nanowire single photon detectors," *IEEE Transactions on Applied Superconductivity*, Vol. 19, No. 3, pp. 341-345, 2009.

[47] B. Hillerich and A. Geyer, "Self-aligned flat-pack fiber-photodiode coupling," *Electronics Letters*, Vol. 24, No. 15, pp. 918-919, 1988.

[48] D.H. Hartman, M.K. Grace, and F.V. Richard, "An effective lateral fiberoptic electronic coupling and packaging technique suitable for VHSIC applications," *Journal of Lightwave Technology*, Vol. 4, No. 1, pp. 73-82, 1986.

[49] Y. Muramoto, Y. Hirota, K. Yoshino, H. Ito, and T. Ishibashi, "Uni-travelling-carrier photodiode module with bandwidth of 80 GHz," *Electronics Letters*, Vol. 39, No. 25, pp. 1851-1852, 2003.

[50] T. Hiraki, T. Tsuchizawa, H. Shibata, H. Nishi, H. Fukuda, R. Kou, K. Takeda, and K. Yamada, "*Cryogenic Photonic Module Based on Silicon Photonic Wire Waveguides*," *CLEO:* 2013, Optical Society of America, San Jose, CA, 2013.

[51] C. Kopp, S. Bernabé, B.B. Bakir, J.-M. Fedeli, R. Orobtchouk, F. Schrank, H. Porte, L. Zimmermann, and T. Tekin, "Silicon photonic circuits: on-CMOS integration, fiber optical coupling, and packaging," *IEEE Journal of Selected Topics in Quantum Electronics*, Vol. 17, No. 3, pp. 498-509, 2011.

[52] H. Terai, S. Miki, and Z. Wang, "Readout electronics using single-flux-quantum circuit technology for superconducting single-photon detector array," *IEEE Transactions on Applied Superconductivity*, Vol. 19, No. 3, pp. 350-353, 2009.

[53] H. Terai, S. Miki, T. Yamashita, K. Makise, and Z. Wang, "Demonstration of single-flux-quantum readout operation for superconducting single-photon detectors," *Applied Physics Letters*, Vol. 97, No. 11, 112510, 2010.

[54] T. Ortlepp, M. Hofherr, L. Fritzsch, S. Engert, K. Ilin, D. Rall, H. Toepfer, H.-G. Meyer, and M. Siegel, "Demonstration of digital readout circuit for superconducting nanowire single photon detector," *Optics Express*, Vol. 19, No. 19, pp. 18593-18601, 2011.

[55] M. Maruyama, K. Uekusa, T. Konno, N. Sato, M. Kawabata, T. Hato, H. Suzuki, and K. Tanabe, "HTS sampler with optical signal input," *IEEE Transactions on Applied Superconductivity*, Vol. 17, No. 2, pp. 573-576, 2007.

[56] S. Shinada, H. Terai, Z. Wang, and N. Wada, "1550 nm band optical input module with superconducting single-flux-quantum circuit," *Applied Physics Letters*, Vol. 96, No. 18, p. 182504, 2010.

[57] S. Bernabe, C. Kopp, L. Lombard, and J.-M. Fedeli, "Microelectronic-like packaging for silicon photonics: a 10 Gbps multi-chip-module optical receiver based on Ge-on-Si photodiode," Proceedings of the 2010 Third Electronic System-Integration Technology Conference (ESTC), pp. 1-5, Berlin, Germany, 13-16 September 2010.

[58] S. Bernabe, R. Stevens, M. Volpert, R. Hamelin, C. Rossat, F. Berger, L. Lombard, C. Kopp, J. Berggren, P. Sundgren, and M. Hammar, "Highly integrated VCSEL-based 10Gb/s miniature optical sub-assembly," Proceedings of the 55th Electronic Components and Technology Conference, 2005, pp. 1333-13338, 31 May-3 June 2005.

[59] H. Takashima, T. Asai, K. Toubaru, M. Fujiwara, K. Sasaki, and S. Takeuchi, "Fiber-microsphere system at cryogenic temperatures toward cavity QED using diamond NV centers," *Optics Express*, Vol. 18, No. 14, pp. 15169-15173, 2010.

[60] W. Slysz, M. Węgrzecki, J. Bar, P. Grabiec, M. Górska, V. Zwiller, C. Latta, P. Bohi, I. Milostnaya, O. Minaeva, A. Antipov, O. Okunev, A. Korneev, K. Smirnov, B. Voronov, N. Kaurova, G. Gol'tsman, A. Pearlman, A. Cross, I. Komissarov, A. Verevkin, and Roman Sobolewski, "Fiber-coupled single-photon detectors based on NbN superconducting nanostructures for practical quantum cryptography and photon-correlation studies," *Applied Physics Letters*, Vol. 88, No. 26, 261113, 2006.

[61] A.J. Miller, A.E. Lita, B. Calkins, I. Vayshenker, S.M. Gruber, and S.W. Nam, "Compact cryogenic self-aligning fiber-to-detector coupling with losses below one percent," *Optics Express*, Vol. 19, No. 10, pp. 9102-9110, 2011.

[62] S. Miki, M. Takeda, M. Fujiwara, M. Sasaki, and Z. Wang, "Compactly packaged superconducting nanowire single-photon detector with an optical cavity for multichannel system," *Optics Express*, Vol. 17, No. 26, pp. 23557-23564, 2009.

[63] S. Miki, T. Yamashita, M. Fujiwara, M. Sasaki, and Z. Wang, "Multi-channel SNSPD system with high detection efficiency at telecommunication wavelength," *Optics Letters*, Vol. 35, No. 13, pp. 2133-2135, 2010.

[64] R.H. Shepard, A. Guzman, M.E. Grein, E.A. Dauler, D. Rosenberg, T. Gudmundsen, and R.P. Murphy, "A robust optical coupler for alignment of superconducting nanowire detector array," *CLEO: QELS_Fundamental Science*, Optical Society of America, San Jose, CA, 2015.

[65] K. Yoshino, Y. Muramoto, T. Furuta, and H. Ito, "High-speed uni-travelling-carrier photodiode module for ultra-low temperature operation," *Electronics Letters*, Vol. 41, No. 18, pp. 1030-1031, 2005.

[66] H. Suzuki, "Evaluation of uni-traveling carrier photodiode performance at low temperatures and applications to superconducting electronics," in *Photodiodes - Communications, Bio-Sensings, Measurements and High-Energy Physics,* Jin-Wei Shi (Ed.) [Online]. ed. http://www.intechopen.com/books/photodiodes-communications-bio-sensings-measurements-and-high-energy-physics/evaluation-of-uni-traveling-carrier-photodiode-performance-at-low-temperatures-and-applications-to-s, 2011.

[67] J.F. Bulzacchelli, H.-S. Lee, K.G. Stawiasz, S. Alexandrou, and M.B. Ketchen, "Picosecond optoelectronic study of superconducting microstrip transmission lines," *IEEE Transactions on Applied Superconductivity*, Vol. 5, No. 2, pp. 2839-2843, 1995.

[68] X. Hu, T. Zhong, J.E. White, E.A. Dauler, F. Najafi, C.H. Herder, F.N.C. Wong, and K.K. Berggren, "Fiber-coupled nanowire photon counter at 1550 nm with 24% system detection efficiency," *Optics Letters*, Vol. 34, No. 23, pp. 3607-3609, 2009.

[69] C.A. Clayton, "The implications of image scrambling and focal ratio degradation in fiber optics on the design of astronomical instrumentation," *Astronomy and Astrophysics*, Vol. 213, No. 1-2, pp. 502-515, 1989.

Downloaded from http://meridian.allenpress.com/imaps/article-pdf/12/4/189/2245811/imaps_485.pdf by guest on 31 October 2022

[70] D. Lee, R. Haynes, and D.J. Skeen, "Properties of optical fibres at cryogenic temperatures," *Monthly Notices of the Royal Astronomical Society*, Vol. 326, No. 2, pp. 774-780, 2001.
[71] K.E. Bean, "Anisotropic etching of silicon," *IEEE Transactions on Electron Devices*, Vol. 25, No. 10, pp. 1185-1193, 1978.
[72] C.W. Tan, Y.C. Chana, H.P. Chana, N.W. Leung, and C.K. So, "Investigation on bondability and reliability of UV-curable adhesive joints for stable mechanical properties in photonic device packaging," *Microelectronics and Reliability*, Vol. 44, No. 5, pp. 823-831, 2004.
[73] A. Priyadarshi, L.H. Fen, S.G. Mhaisalkar, V. Kripesh, and A.K. Asundi, "Fiber misalignment in silicon V-groove based optical modules," *Optical Fiber Technology*, Vol. 12, No. 2, pp. 170-184, 2006.
[74] S.Q. Ou, G. Xu, Y. Xu, and K.N. Tu, "Optical fiber packaging by lead (Pb)-free solder in V-grooves," *Ceramics International*, Vol. 30, No. 7, pp. 1115-1119, 2004.
[75] D.C. Abeysinghe, V. Ranatunga, A. Balagopal, H. Mu, K. Ye, and D. Klotzkin, "A novel technique for high-strength direct fiber-to-Si submount attachment using field-assisted anodic bonding for optoelectronics packaging," *IEEE Photonics Technology Letters*, Vol. 16, No. 9, pp. 2150-2152, 2004.
[76] G. Pubanz, *Cryogenic Optical/Electrical Interconnect Module*, Google Patents, Tektronix, Inc, 2000.
[77] E. Suhir, "Thermal stress failures in electronics and photonics: physics, modeling, prevention," *Journal of Thermal Stresses*, Vol. 36, No. 6, pp. 537-563, 2013.
[78] G.K. White, "Thermal expansion of reference materials: copper, silica and silicon," *Journal of Physics. D, Applied Physics*, Vol. 6, No. 17, p. 2070-2078, 1973.
[79] N. Bouras, M.A. Madjoubi, M. Kolli, S. Benterki, and M. Hamidouche, "Thermal and mechanical characterization of borosilicate glass," *Physics Procedia*, Vol. 2, No. 3, pp. 1135-1140, 2009.
[80] G. Schwarz, "Thermal expansion of polymers from 4.2 K to room temperature," *Cryogenics*, Vol. 28, No. 4, pp. 248-254, 1988.
[81] U. Escher, "Thermal eExpansion of epoxy resins with different cross-link densities at low temperatures," *Cryogenics*, Vol. 35, No. 11, pp. 775-778, 1995.
[82] S. Usami, H. Ejima, T. Suzuki, and K. Asano, "Cryogenic small-flaw strength and creep deformation of epoxy resins," *Cryogenics*, Vol. 39, No. 9, pp. 729-738, 1999.
[83] S. Van Sciver, "Low-temperature materials properties", *Helium Cryogenics*., Springer, New York, pp. 17-58, 2012.
[84] D. Xue, T. Yanhong, and Z. Xin, "Mechanical properties and microstructure of Sn-based solder joints at cryogenic temperature," Proceedings of the 2014 15th International Conference on Electronic Packaging Technology (ICEPT), pp. 888-892, Chengdu, China, 12-15 August 2014.
[85] S. Nishijima, Y. Honda, and T. Okada, "Application of the positron annihilation method for evaluation of organic materials for cryogenic use," *Cryogenics*, Vol. 35, No. 11, pp. 779-781, 1995.
[86] S.W. Park and D.G. Lee, "Strength of double lap joints bonded with carbon black reinforced adhesive under cryogenic environment," *Journal of Adhesion Science and Technology*, Vol. 23, No. 4, pp. 619-638, 2009.
[87] C.J. Huang, S.Y. Fu, Y.H. Zhang, B. Lauke, L.F. Li, and L. Ye, "Cryogenic properties of SiO2/epoxy nanocomposites," *Cryogenics*, Vol. 45, No. 6, pp. 450-454, 2005.
[88] J.P. Yang, G. Yang, G. Xu, and S.-Y. Fu, "Cryogenic mechanical behaviors of MMT/epoxy nanocomposites," *Composites Science and Technology*, Vol. 67, No. 14, pp. 2934-2940, 2007.
[89] I.F. Silvera, A. Abate, A. Chijioke, and A. Pashin, "Adhesives for highly polished surfaces and low temperature: a simple test and results," *The Review of Scientific Instruments*, Vol. 73, No. 5, pp. 2108-2114, 2002.
[90] B.P. Solano, *Cryogenic Silicon Microstrip Detector Modules for the LHC*, Universitat Politècnica de Catalunya, Escola Tècnica Superior d'Enginyeria Industrial de Barcelona ETSEIB, Barcelona, Spain, 2004.
[91] K.E. Hokanson and A. Barcohen, "A shear-based optimization of adhesive thickness for die bonding," *IEEE Transactions on Components Packaging and Manufacturing Technology Part A*, Vol. 18, No. 3, pp. 578-584, 1995.
[92] C.S. Bang, J.G. Kim, and D.G. Lee, "Cryogenic performance of adhesively bonded metal joints for LNG containment system," *Journal of Adhesion Science and Technology*, Vol. 26, No. 7, pp. 969-986, 2012.
[93] D. Wu, Y.C. Lee, and P. Masterson, "Reliability study of an epoxy-bonded laser-to-fiber assembly," Proceedings of the 48th IEEE Electronic Components and Technology Conference, 1998, pp. 1186-1191, Seattle, WA, 25-28 May 1998.
[94] H.M. Oluseyi, J.H. Bercovitz, A. Karcher, C.D. Hernikl, T. Miller, M. Uslenghi, N. Roe, C. Bebek, S.E. Holland, and M.E. Levi, "LBNL four-side buttable CCD package development," Proceedings of Electronic Imaging 2004, pp. 87-98, Bellingham, WA, 2004.
[95] D. Vukobratovich, K.A. Fetterhoff, J.R. Myers, P.D. Wheelwright, and G.R. Cunnington, "Bonded mounts for small cryogenic optics." Proceedings of the International Symposium on Optical Science and Technology, pp. 228-239, 2000.
[96] A. Cremonini, S. Mariotti, and J. Roda, "An overview on packaging of microwave electronic devices operating in a cryogenic environment," *Cryogenics*, Vol. 52, No. 10, pp. 445-451, 2012.
[97] S.G. Kang, M.G. Kim, and C.G. Kim, "Evaluation of cryogenic performance of adhesives using composite-aluminum double-lap joints," *Composite Structures*, Vol. 78, No. 3, pp. 440-446, 2007.
[98] R.R. Tummala, *Fundamentals of Microsystems Packaging*, McGraw Hill, New York, 2001.
[99] B.C. Kim, S.W. Park, and D.G. Lee, "Fracture toughness of the nano-particle reinforced epoxy composite," *Composite Structures*, Vol. 86, No. 1-3, pp. 69-77, 2008.
[100] Epoxy Technology Inc., "Cure matters—determining the proper cure schedule," Epoxy Technology Inc., Billerica, MA, [Online]. http://www.epotek.com/site/files/brochures/pdfs/Cure_Matters_Final.pdf, Accessed August 2015.
[101] K.H. Lee and D.G. Lee, "Smart cure cycles for the adhesive joint of composite structures at cryogenic temperatures," *Composite Structures*, Vol. 86, No. 1-3, pp. 37-44, 2008.
[102] T. Hayashi, "An innovative bonding technique for optical chips using solder bumps that eliminate chip positioning adjustments," *IEEE Transactions on Components Hybrids and Manufacturing Technology*, Vol. 15, No. 2, pp. 225-230, 1992.
[103] Z. Tang, T. Shi, and F.G. Shi, "Advanced packaging of optoelectronic devices," *Wiley Encyclopedia of Electrical and Electronics Engineering*, John Wiley & Sons, Inc., New York, 2001.
[104] R.K. Kirschman, W.M. Sokolowski, and E.A. Kolawa, "Die attachment for-120 degrees C to +20 degrees C thermal cycling of microelectronics for future mars rovers: an overview," *Journal of Electronic Packaging*, Vol. 123, No. 2, pp. 105-111, 2001.
[105] T. Ogashiwa, H. Nakagawa, H. Akimoto, H. Shigyo, and S. Takada, "Flip-chip bonding using superconducting solder bump," *Japanese Journal of Applied Physics*, Vol. 34, No. 8A, pp. 4043-4046, 1995.
[106] C.J. Burroughs, S.P. Benz, P.D. Dresselhaus, Y. Chong, and H. Yamamori, "Flexible cryo-packages for Josephson devices," *IEEE Transactions on Applied Superconductivity*, Vol. 15, No. 2, pp. 465-468, 2005.
[107] K.E. Yokoyama, G. Akerling, A.D. Smith, and M. Wire, "Robust superconducting die attach process," *IEEE Transactions on Applied Superconductivity*, Vol. 7, No. 2, pp. 2631-2634, 1997.
[108] Y. Hashimoto, S. Yorozu, T. Satoh, and T. Miyazaki, "Demonstration of chip-to-chip transmission of single-flux-quantum pulses at throughputs beyond 100 Gbps," *Applied Physics Letters*, Vol. 87, No. 2, 022502, 2005.
[109] S.B. Kaplan, V. Dotsenko, and D. Tolpygo, "High-speed experimental results for an adhesive-bonded superconducting multi-chip module," *IEEE Transactions on Applied Superconductivity*, Vol. 17, No. 2, pp. 971-974, 2007.
[110] R.S.E. John, A.P. Malshe, V. Dotsenko, J. Delmas, R. Webber, and D. Gupta, "Nano-integrated adhesive for cryogenic packaging (4K) of harsh environment electronics," Proceedings of the 60th Electronic Components and Technology Conference (ECTC), pp. 960-966, Las Vegas, NV, 1-4 June 2010.
[111] R.S.E. John, C.S. Thompson, V.V. Dotsenko, J. Delmas, A.P. Malshe, and D. Gupta, "Carbon nanotube based polymer adhesive as an underfill for superconductor multi-chip module packaging," *IEEE Transactions on Applied Superconductivity*, Vol. 21, No. 3, pp. 900-903, 2011.
[112] R.W. Chang and F.P. McCluskey, "Reliability assessment of indium solder for low temperature electronic packaging," *Cryogenics*, Vol. 49, No. 11, pp. 630-634, 2009.
[113] S. Narayana, V.K. Semenov, Y.A. Polyakov, V. Dotsenko, and S.K. Tolpygo, "Design and testing of high-speed interconnects for superconducting multi-chip modules," *Superconductor Science and Technology*, Vol. 25, No. 10, 105012, 2012.

Downloaded from http://meridian.allenpress.com/jmep/article-pdf/12/4/189/2245811/imaps_485.pdf by guest on 31 October 2022